

ALMA MATER STUDIORUM · UNIVERSITÀ DI  
BOLOGNA

---

Scuola di Scienze  
Corso di Laurea Magistrale in Fisica

**Entropic forces  
and dynamical properties of a  
rigid body Boltzmann gas**

**Relatore:**  
**Prof. Armando Bazzani**

**Presentata da:**  
**Andrea Cerfogli**

**Sessione II**  
**Anno Accademico 2017/2018**



# Contents

<b>1</b>	<b>Introduction</b>	<b>5</b>
<b>2</b>	<b>Entropic Force Theory</b>	<b>9</b>
2.1	Force Method . . . . .	10
2.2	Extended Gibbs Adsorption Equation Method . . . . .	12
2.3	Derjaguin Approximation . . . . .	17
<b>3</b>	<b>Effects of a Boltzmann Gas</b>	<b>21</b>
<b>4</b>	<b>Program and Simulations</b>	<b>31</b>
4.1	Not Only Colliding Spheres . . . . .	31
4.2	Effects of the Excluded Volume . . . . .	35
4.2.1	Determination of the Potential . . . . .	36
4.2.2	Estimation of the Clustering Time . . . . .	44
<b>5</b>	<b>Conclusive Remarks</b>	<b>53</b>
<b>A</b>	<b>Recent experimental discoveries</b>	<b>55</b>
A.1	Molecules and temperature gradient . . . . .	55



# Chapter 1

## Introduction

In this thesis project we study, simulate and analyse the issue of entropic forces and their effects in a simple gaseous system. This project focuses on the aspect of the effect of these forces in dynamical situations.

This thesis project started because after a long talk with my supervisor and following with some more detailed readings [2, 3], I was fascinated by his idea on how life came to be on earth due to uneven forces. In the beautiful idea shown to me, the evolution mechanisms are essentially based on randomness and we have some paradoxes to understand how it was possible to select the amino acid sequence of a protein that define its three-dimensional structure essential for the metabolism processes of life. The role of entropic forces could shed light on the problem.

We are still far from achieving meaningful results about this concept, but we have made the first steps in the direction obtained from such an interesting idea.

The starting point of this project is the effects of entropic or depletion forces and they mainly concern colloids. Let's define what colloids are. Following the IUPAC's definition the term colloidal refers to a state of subdivision, implying that the particles dispersed in a medium, either liquid or gaseous, have at least in one direction a dimension approximately between  $10^{-9} m$  and  $10^{-6} m$  or that in a system discontinuities are found at distances of that order. Colloids are quite bigger compared to normal molecules, but they may be comparable to the size of macromolecules.

We want now to give an insight to the reader to what entropic forces are through a real life mental experiment. Let us consider a room in a restaurant in two different occasions. On regular evenings the tables are arranged in a normal dinner set-up. Sometimes they set up a cocktail party with many people present. In such an event the tables are full of snacks and beverages and the arrangement of the tables is quite different. When the number of

costumers increases and get over a certain threshold, the staff tend to push the table close to each other in order to get more free space for the visitors. This is a kind of 'phase separation' and is triggered by entropy only. We see an apparent attraction between the tables that originates from repulsive interaction between the customers, which do not wish to be too close each other. If we think of the tables as a colloidal particles in a solution, and the costumers as smaller particles, we have the gist of how entropic forces work.

In fact if we suppose that rigid colloidal sphere are mixed with smaller rigid polymeric spheres the bigger ones have a portion of excluded volume, i.e. 'void' space near the surface in which the smaller particles cannot enter. The mechanism that is responsible for attraction originates from the superimposition of two of this layers from different colloidal particles: when two layers superimpose the space available to the smaller particles increases. It follows that the free energy of the smaller spheres is minimised by states in which the big spheres are close together. The visible effect is an attractive force between the bigger spheres even if the only interactions are repulsive of non superposition. Instead, in the entropic picture, we have that it is more probable to find two big spheres close one to the other due to the effect of the smaller spheres, because this increase the free volume available for the smaller spheres and this increases the total entropy of the system. For small concentrations the attraction is equal to the product of the osmotic pressure and the overlap volume. Moreover we have a discontinuous behaviour, which is typical in a model where elastic collision between rigid object happens.

The concept of entropic force was first derived by Asakura and Oosawa in 1954 [1]. In the first chapter of this thesis project we will present how the understanding of this concept came to be, retracing the steps made by the discoverers of this force. We show from a very simple geometrical calculation how the entropic forces are derived between two plates, which is very straightforward, between two spheres and between a wall and a sphere. We want to highlight that Asakura and Oosawa demonstrated theoretically the existence of this force, but we focused on the dynamical effect of this forces.

In the second chapter we decided to look into a different effect of excluded volumes through a new idea developed by us. In fact we still don't know with precision how they act in many situation, in particular which is their role in many situation of non-equilibrium.

The shape of the proteins or of other molecules determines the forces, due to the excluded volume, to which they are subjected. For a better understanding we calculate how a two dimensional hypothetical rigid molecule, with a non symmetrical shape, behaves when hit by a beam of small particles with a not null volume.

The molecule is split in two along an axis of non symmetry and the beam

of particles are carrying a momentum only in the direction perpendicular to that axis, the particles from the beam arrive both from  $+\infty$  and  $-\infty$ .

The cross section of the molecule in the two different direction cover the same area, but due to the different shape of the molecule and to the fact that the particles have a volume and are not point-like, the value of the momentum at each height is different, and is in function of the radius of the particles.

In the third chapter we tried to obtain computational result through simulations of a gas in different systems. In the chapter dedicated to the simulation we give to the reader a brief explanation on how the program *Not Only Colliding Spheres* (NOCS), written in the language C++, works. NOCS is a program able to reproduce the dynamics of molecules in two dimension.

In this thesis project we used NOCS to reproduce, as a first step, the result obtained by [8], who used a Monte Carlo simulation for obtaining the shape of the entropic potential. We were able to reproduce the same shape of the potential through a dynamical simulation.

We want to highlight that the simulations done with NOCS are original endeavour developed by us.

A different simulation we focused on, is one in which we studied the distribution of the time intervals in which the particles kept close one to each other. This is important because in physics, in biology and in chemistry many reaction happen only if the time two particles or molecules spend together is long enough.

The shape of the distribution of the time length is exponential and we obtained interesting data that connects the depth of the potential well obtained in the previous simulation with the coefficient of the exponential distribution of time length two particles stay close together.

Afterwards we decided to present to the reader, in the appendix, some recent experimental discoveries on the Soret effect, for which particles in aqueous solutions usually move from regions with higher temperature to regions with lower temperature, [4, 5]. The Soret effect theoretically is not yet clearly understood, since there are many different elements which contribute and as it can happens in effects due to thermodynamic which are often complex.

The authors, using lasers to heat a film of water will create a gradient of temperature in the film enclosed by polystyrene slides. Afterwards through

It will be shown that if the system is sufficiently steady, i.e. not too hot, and the the Soret coefficient is linked to the entropy.



## Chapter 2

# Entropic Force Theory

Asakura and Oosawa [1] deduced an attractive force acting between suspended colloids in a solution of polymeric particles, which act as depletants, where there is neither direct interaction between two colloids nor between colloids and solute polymeric particles. This force has a range of interaction of the order of the diameter of the polymeric particle and a magnitude of the osmotic pressure of the polymeric particles.

In their article Asakura and Oosawa approximate the bigger colloids and the smaller polymeric particles as rigid spheres with two different radii, the size of the two kind of spheres is the only difference between them.

The polymeric particles compete with the bigger colloidal particle to have access to the available volume, decreasing it, and in this sense the colloidal particles are called depletants. Since the colloids have less volume available, they are more likely to be close to each other compared to if there were only the same number of colloids in the same volume.

When two colloids get close enough, closer than two times the radius of the small polymeric particles, the smaller particles apply a force to the two colloids, force caused by an unbalanced osmotic pressure, but since the force is small and in a gas mixture is present a lot of thermal noise, the colloids tends to wander off. However since the colloids perceive a force they spend more time close to each other and since time is required to trigger many biochemical reactions, depletion forces play an important role in nature.

In the following chapter we want to highlight the most important steps done in the description of the depletion forces. In the following theoretical derivation the colloids considered will be blocked in place, because it is not easy to obtain a direct dynamic derivation of the depletion forces. This thesis projects revolves more on the dynamical aspect of the depletion interactions however it is relevant to learn from the work of Asakura and Oosawa since their work started all the further derivations.

## 2.1 Force Method

### Entropic Interaction Between two Flat Plates

Let us consider two large parallel plates immersed in a solution of rigid spherical polymeric particles. If the distance between the inner surfaces of these two plates is smaller than the diameter of solute polymeric particles, none of those polymeric particles can enter in the space between the plates. Therefore a force equivalent to the osmotic pressure of the solution of polymeric particles acts on the outer surfaces of these plates.

The force per unit area,  $K(h)$ , between the two parallel plates separated by a distance  $h$ , is the difference between the osmotic pressure  $P_i$  inside the plates and the outside pressure  $P_o$

$$K = P_i - P_o . \quad (2.1.1)$$

We suppose that the hard spheres behave thermodynamically ideally and so the osmotic pressure outside the plates is given by Van't Hoff law

$$P_o = n_b kT,$$

where  $n_b$  is the bulk number density of the polymers. When the plate separation  $h$  is equal or larger than the diameter  $\sigma$  of the hard spheres the osmotic pressure inside the plates is equal to the one outside:

$$P_i = P_o = n_b kT,$$

Instead when  $h$  is smaller than  $\sigma$  no polymer can enter the gap and  $P_i = 0$ . Summarising the last results we have:

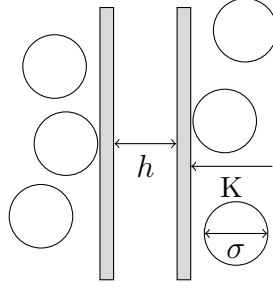
$$\begin{aligned} K(h) &= -n_b kT & \text{for } h < \sigma \\ &= 0 & \text{for } h \geq \sigma . \end{aligned} \quad (2.1.2)$$

As we can see from the last equation, we have a discontinuous behaviour, this is typical in a model where we have elastic collision between rigid object.

We know that  $K = -dW/dh$ , and integrating from  $\infty$  to  $h$  yields the interaction potential per unit area  $W(h)$  between the plates at distance ( $h$ )

$$\begin{aligned} W(h) &= -n_b kT(\sigma - h) & \text{for } h < \sigma \\ &= 0 & \text{for } h \geq \sigma . \end{aligned} \quad (2.1.3)$$

Figure 2.1:  
Schematic picture  
of two parallel  
flat plates in the  
presence of hard  
spheres



## Entropic Interaction Between two Spheres in two dimensions

When the volume of thickness  $\sigma/2$  around the spherical colloidal particles with radius  $R$  start to overlap, i.e. when the distance  $r$  between the centres of the two colloidal particles is smaller than  $2R + \sigma$ , a clear force arises between these colloidal particles. Let's define an effective entropic force radius  $R_e$

$$R_e = R + \frac{\sigma}{2} . \quad (2.1.4)$$

This attractive force originates from an uncompensated osmotic pressure due to the diminution of the available volume between the colloidal particles.

We can see in the Fig. 2.2 that the uncompensated pressure acts on the surface from  $\theta = 0$  to  $\theta = \theta_0$ ,  $\theta_0 = \arccos(r/2R_e)$ .

For symmetry reasons only the contributes to the total force along the line who connects the two spheres is meaningful. The angle on which this forces operate is between  $\theta$  e  $\theta + d\theta$ , whose surface is  $2\pi R_e^2 \sin(\theta)d\theta$  We can obtain the whole force acting between the colloidal spheres integrating from 0 to  $\theta_0$  on  $\theta$

$$\begin{aligned} \frac{K_s(r)}{n_b k T} &= -2\pi \left(R + \frac{\sigma}{2}\right)^2 \int_0^{\theta_0} \sin\theta \cos\theta \, d\theta \\ &= -\pi R_e^2 \left[1 - \left(\frac{r}{2R_e}\right)^2\right] & 2R \leq r < 2R_e \\ &= 0 & r \geq 2R_e . \end{aligned} \quad (2.1.5)$$

The minus sign in the last equations stand for an attractive force.

We can now obtain a depletion potential by integration of the depletion force

$$\begin{aligned}
W_s(r) &= \int_r^{2R_e} K_s(r) dr \\
&= -n_b k T V_{ov}(r) \quad 2R \leq r < 2R_e \\
&= 0 \quad r \geq 2R_e .
\end{aligned} \tag{2.1.6}$$

We can note that the potential  $W_s(r)$  is equal to pressure time the overlap volume  $V_{ov}$  where

$$V_{ov}(r) = \frac{4\pi}{3} R_e^3 \left[ 1 - \frac{3}{4} \frac{r}{R_e} + \frac{1}{16} \left( \frac{r}{R_e} \right)^3 \right] \tag{2.1.7}$$

or can be expressed as follows

$$V_{ov}(h) = \frac{\pi}{6} (\sigma - h)^2 \left( 3R + \sigma + \frac{h}{2} \right) . \tag{2.1.8}$$

Both equations are widely used in the literature.

In the limit  $\sigma/2 \ll R$  the force expressed in equ. (2.1.5) becomes

$$\frac{K_s(h)}{n_b k T} = -\pi R (\sigma - h) \tag{2.1.9}$$

and from the potential (2.1.6) we get

$$\frac{W_s(h)}{n_b k T} = -\pi \frac{R}{2} (\sigma - h)^2 . \tag{2.1.10}$$

The latter two formulae are valid when  $h = r - 2R < \sigma$ .

## 2.2 Extended Gibbs Adsorption Equation Method

### Entropic interaction between two flat plates

An alternative way to obtain the interaction potential is from the extended Gibbs adsorption equation. We use the gran potential  $\Omega(T, V, \mu, h)$  as the best thermodynamic potential able to describe the situation in Fig. 2.3.

$$\Omega = F - \mu N, \tag{2.2.1}$$

where  $F = F(T, V, N, h)$  is the Helmholtz free energy,  $N$  the number of hard spheres in the system and  $\mu$  their chemical potential. We have that at a constant temperature and volume  $dF = \mu dN - K A dh$ , so

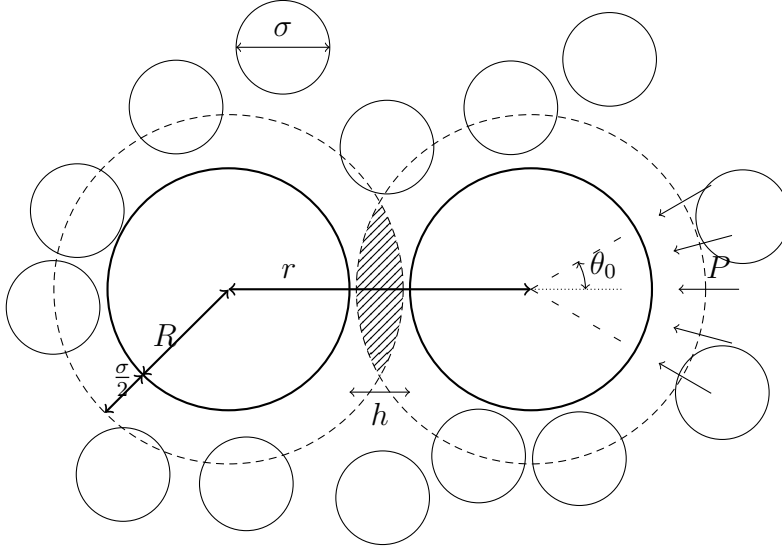


Figure 2.2: Two hard spheres in the presence of smaller hard spheres as depletants. The proximity of the two spheres produce an overlap of areas (grey part) excluded to the centre of the smaller spheres, resulting in more free space for the smaller spheres. The overlapped area has the shape of a lens with thickness  $\sigma - h$  and height  $H = 2R_e \tan \theta_0$ , where  $\theta_0$  is give by  $\cos \theta_0 = r/2R_e$ . The unbalanced number of strikes for the bigger spheres causes an unbalanced pressure  $P$ , resulting in an attractive force between them.

$$d\Omega = -KAdh - Nd\mu, \quad (2.2.2)$$

where  $K$  is the force per unit area between the plates and  $A$  is the area of the plates. Differentiating the previous equation we obtain

$$\left(\frac{\partial K}{\partial \mu}\right)_h = \frac{1}{A} \left(\frac{\partial N}{\partial h}\right)_\mu \quad (2.2.3)$$

knowing that

$$K = - \left(\frac{\partial W}{\partial h}\right)_\mu, \quad (2.2.4)$$

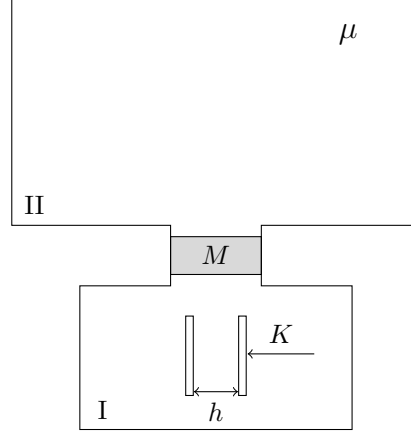
we get that

$$- \left(\frac{\partial}{\partial h} \left(\frac{\partial W}{\partial \mu}\right)_h\right)_\mu = \frac{1}{A} \left(\frac{\partial N}{\partial h}\right)_\mu \quad (2.2.5)$$

The depletion potential  $W$  vanishes at infinite separation for all values of  $\mu$  of the depletion agent, integrating over  $h$  bring us

$$- \left(\frac{\partial W}{\partial \mu}\right)_h = \frac{N(h) - N(\infty)}{A}, \quad (2.2.6)$$

Figure 2.3: Illustration on how the entropic forces between two plates in the system of interest (I) at the given chemical potential of the reservoir (II). The two systems are connected by a membrane  $M$  able to let go through the particles of the depletants



where  $N(h)$  is the number of hard spheres in the system when the plates are at separation  $h$  and  $N(\infty)$  is that at infinite separation. We can express the number of hard spheres in the previous equation in terms of the surface adsorption

$$\left(\frac{\partial W}{\partial \mu}\right)_h = \Gamma(h) - \Gamma(\infty), \quad (2.2.7)$$

where

$$\Gamma(h) = \int_0^h (n(x) - n_b) dx, \quad (2.2.8)$$

and

$$\Gamma(\infty) = 2\Gamma_{single\ wall} = 2 \int_0^\infty (n(x) - n_b) dx. \quad (2.2.9)$$

In equ. (2.2.9)  $n(x)$  refers to the concentration profile of spheres near a single wall, while in equ. (2.2.8)  $n(x)$  we have the profile between two walls. Expression (2.2.7) is the extension of the Gibbs adsorption equation for a single surface to the case of two surfaces at finite separation. Integration of equ (2.2.7) gives

$$W(h) = - \int_{-\infty}^{\mu} (\Gamma(x) - \Gamma(\infty)) d\mu. \quad (2.2.10)$$

The centre of the hard spheres can't get closer to the wall of the plate than  $\sigma/2$  and  $A\Gamma(h)$  is equal to the overlap volume  $A(\sigma - h)$  times  $n_b$ , as shown in Fig. 2.4.

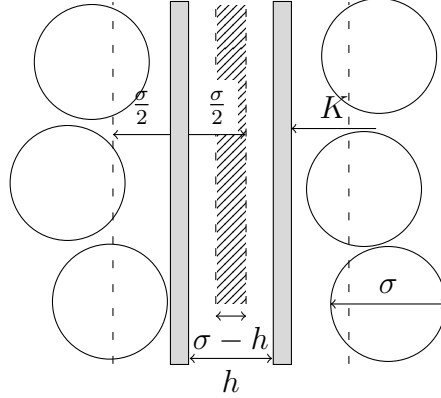


Figure 2.4: The overlap volume (hatched area) due to hard spheres between two parallel flat plates equals to  $A(\sigma - h)$

$$\begin{aligned} \Gamma(h) - \Gamma(\infty) &= n_b(\sigma - h) \quad \text{for } h < \sigma \\ &= 0 \quad \text{for } h \geq \sigma \end{aligned} \quad (2.2.11)$$

The chemical potential of the hard spheres is

$$\mu = kT \ln(n_b). \quad (2.2.12)$$

If we insert equations (2.2.11) and (2.2.12) into equ. (2.2.10) we find again the interaction given by equ. (2.1.3). The calculation with the extended Gibbs adsorption equation has a conceptual advantage, it provides a direct link between the depletion of particles with the entropic potential. This method also gives us a physically motivated approximate expression for the entropic interaction where an exact calculation is not possible.

## Interaction Potential Between two Spheres

Applying exactly the same line of reasoning as for the derivation of the extended Gibbs adsorption equation for two flat plates, now we obtain

$$-\left(\frac{\partial W_s}{\partial \mu}\right) = N(r) - N(\infty), \quad (2.2.13)$$

where  $N(r)$  is the number of penetrable hard spheres in the system when the colloidal spheres are centre-to-centre separation  $r$  and  $N(\infty)$  at infinite separation. The difference between the two is caused by the overlapping volume of the depletion zones.

$$\begin{aligned} N(r) - N(\infty) &= n_b V_{ov}(r) & \text{for } 2R \leq r < 2R_e \\ &= 0 & \text{for } r \geq 2R_e \end{aligned} \quad (2.2.14)$$

with  $V_{ov}$  defined as in equation (2.1.7) or in (2.1.8). Integrating equ. (2.2.13), while keeping in consideration equations (2.2.14) and (2.2.12) we immediately obtain equ. (2.1.6).

## Interaction Between a Sphere and a Wall

We can apply the extended Gibbs adsorption equation to the case of a sphere interacting with a wall, we use again

$$- \left( \frac{\partial W_{sw}}{\partial \mu} \right) = N(h) - N(\infty), \quad (2.2.15)$$

where  $N(h)$  is the number of penetrable hard spheres in the system when the colloidal sphere is at a separation  $h$  from the wall and  $N(\infty)$  is that at infinite distance. Again the difference between the two are caused by the overlap of the excluded volumes, in this case, of the sphere and the wall (see Fig. 2.5)

$$\begin{aligned} V_{ov}(h) &= \frac{N(h) - N(\infty)}{n_b} \\ &= \frac{1}{3} \pi (\sigma - h)^2 \left( 3R + \frac{\sigma}{2} + h \right) & \text{for } 0 \leq h < \sigma \\ &= 0 & \text{for } h \geq \sigma. \end{aligned} \quad (2.2.16)$$

If we integrate equ. (2.2.15) we get

$$\begin{aligned} \frac{W_{sp}(h)}{n_b k T} &= -\frac{1}{3} \pi (\sigma - h)^2 \left( 3R + \frac{\sigma}{2} + h \right) & \text{for } 0 \leq h < \sigma \\ &= 0 & \text{for } h \geq \sigma. \end{aligned} \quad (2.2.17)$$

When  $R \gg \sigma$  equ. (2.2.17) becomes

$$W_{sp}(h) = -n_b k T \pi R (\sigma - h)^2 \quad \text{for } 0 \leq h < \sigma, \quad (2.2.18)$$

which is equal to two times equ. (2.1.10).

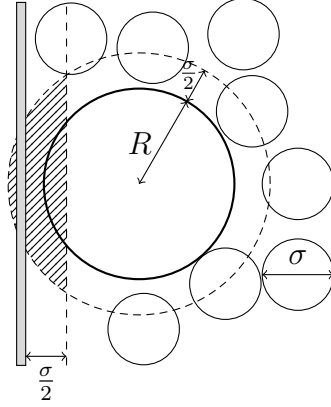


Figure 2.5: Illustration of the overlap volume (hatched) of depletion layers between hard wall and a hard sphere

## 2.3 Derjaguin Approximation

Derjaguin showed an approximate relation for the force between curved object and the interaction potential between two flat plates. In the Derjaguin approximation the spherical surface is replaced by a collection of flat rings. Consider two spheres with radius  $R$  at a centre to centre distance  $r = 2R + h$ . The distance  $H$  between the sphere surfaces at a distance  $z$  from the line joining the centres is  $H = h + 2\Delta$ , we have that  $(R - \Delta)^2 + z^2 = R^2$ , as we can see in Fig. 2.6 (a).

When the range of interaction is short enough it is sufficient to consider only small values of  $h/R$  or  $z/R$ . For  $z \ll R$  since we have

$$\Delta^2 - 2R\Delta + z^2 = 0,$$

from the previous equation, we can solve it for  $\Delta$  and get

$$\Delta_{1,2} = R \pm \sqrt{R^2 - z^2} = R \pm R\sqrt{1 - \frac{z^2}{R^2}}.$$

Since  $z \ll R$  we can expand the root with a Taylor series and truncate the values at the first order, obtaining

$$\Delta_{1,2} = R \pm R \left( 1 - \frac{z^2}{2R^2} \right).$$

We can exclude the value of sigma close to  $2R$ , since it is not the physics condition that interest us, and we get

$$\Delta = \frac{z^2}{2R}.$$

Therefore  $H = h + \frac{z^2}{R}$  and we have that  $dH = (2z/R) dz$ . The interaction between two spheres can be written as the integration of the interactions of flat rings with radius  $z$  and surface  $2\pi z dz$  at a distance  $H(z)$  from each other. If the interaction happens at a suitable short distance, the contributions of the outer rings, with a higher value of  $H$  can be neglected, and so we may extend to  $z = \infty$ .

We have

$$W_s(h) = \int_0^{\infty} W(H) 2\pi z dz = \pi R \int_h^{\infty} W(H) dH \quad (2.3.1)$$

and then

$$K_s = -\frac{\partial W_s(h)}{\partial h} = \pi R W(h), \quad (2.3.2)$$

where in this formula  $W(h)$  is a interaction potential between two flat plates and  $h$  is the distance between the two plates.

The larger the radius of the sphere the more accurate the Derjaguin Approximation is. This approximation is an useful tool which can be very accurate under the right conditions, but it's better to be careful and to be aware of its limitations.

With respect to the depletion interaction the approximation of the Derjaguin approximation becomes accurate when considering a depletion agent which is small compared to the colloidal sphere. If we apply the Derjaguin approximation to equ. (2.1.3) in the case of hard spheres using equ. (2.3.2) we get on the spot at the equ. (2.1.9).

If we apply the same line of reasoning to the interaction between a sphere and a flat plate we have that  $H = h + \Delta$  and thus  $dH = (z/R) dz$ , this bring us to the following force

$$K_{sp} = 2\pi R W(h). \quad (2.3.3)$$

From equation 2.3.3 it follows that

$$W_{sp}(h) = 2\pi R \int_h^{\infty} W(h') dh'. \quad (2.3.4)$$

For the case of hard spheres as depletion agent this gives us

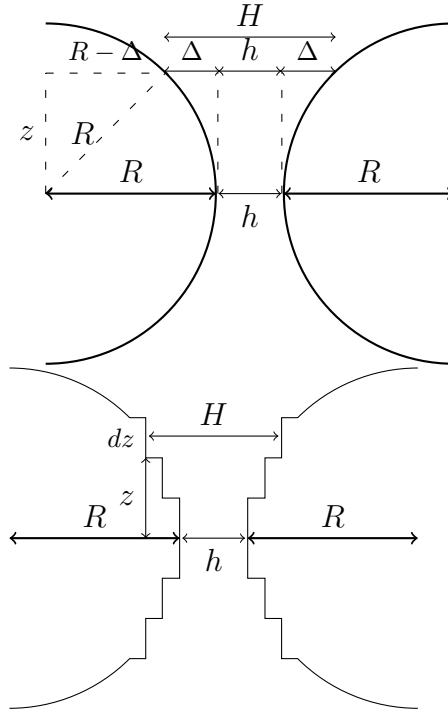


Figure 2.6: How the Derjaguin Approximation works

$$\begin{aligned}
 W_{sp}(h) &= -n_b k T \pi R (\sigma - h)^2 & \text{for } 0 \leq h < \sigma \\
 &= 0 & \text{for } h \geq \sigma,
 \end{aligned}
 \tag{2.3.5}$$

in agreement with equ. (2.2.18).



## Chapter 3

# Effects of a Boltzmann gas on a Molecule

In the first part of this derivation we want to find out how the resultant momentum of a molecule composed of three spheres positioned as in Fig. 3.1, hit by smaller spheres with momentum only in the  $X$  direction, changes in function of  $\sigma$ , the diameter of the smaller spheres. This calculation has been done to understand better the underlying effects of the excluded volume.

Let us consider particles which are evenly distributed along the  $Y$  axis and arrive with a low frequency so that we can suppose the particles have no interaction between them. Let us consider the molecule as set, incapable of moving. When a particle hits a certain sphere of the molecule, we consider that the particle bounces off elastically in the normal direction to the surface of the sphere, as we can see in Fig. 3.2. We will consider in the following calculation that all the smaller spheres carry a momentum in absolute value of  $p_p$ .

When a particle arrives its momentum is given by  $\vec{p}_p = \pm p_p \hat{\mathbf{i}}$ , where  $\hat{\mathbf{i}}$  indicates the unit vector of the  $x$  direction, and the plus or minus sign is determined by which side the particle arrives. After a collision between the particle and the molecule happens the momentum retains his absolute value while his direction changes due to the impact with the molecule. The variation of the momentum of the particle is given by

$$\Delta \vec{p}_p = \vec{p}'_p - \vec{p}_p = \pm p_p \cos \phi \hat{\mathbf{i}} \pm p_p \sin \phi \hat{\mathbf{j}} \pm p_p \hat{\mathbf{i}}, \quad (3.0.1)$$

where  $\hat{\mathbf{j}}$  is the unit vector of the  $y$  direction and the  $\pm$  signs are decided by the quadrant from which the particle arrives and its  $y$  coordinate. The angle  $\phi$  between impact point of a particle and the centre of the sphere of the molecule which was hit is given by

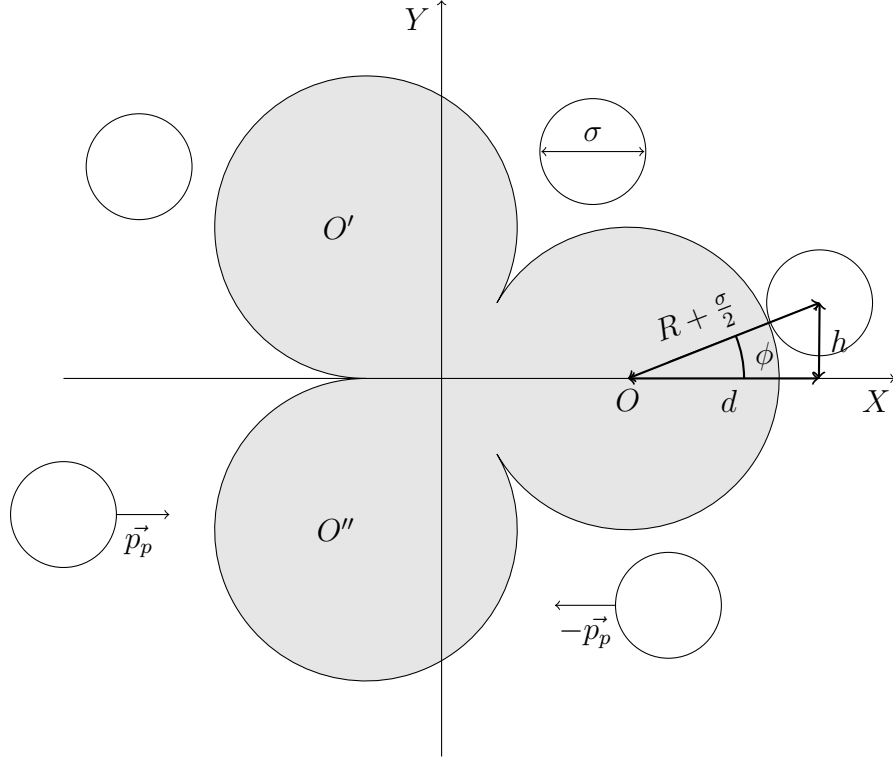


Figure 3.1: The molecule we want to study is composed by the three spheres with their respective centres  $O$ ,  $O'$  and  $O''$ , arranged equally spaced. The angle  $\phi$  is given by the impact point of the molecule and the axis, parallel to the  $X$  axis, passing in the centre of the sphere which has been struck,  $h$  is the relative height of the particle. The sphere-like particles have a diameter of  $\sigma$  and all the particles carry a momentum in absolute value of  $p_p$ , only in the  $X$  direction.

$$\phi(y) = \arctan\left(\frac{h}{d}\right) = \arctan\left(\frac{h}{\sqrt{(R + \frac{\sigma}{2})^2 - h^2}}\right). \quad (3.0.2)$$

Where  $h$  is the relative height at which a particle arrives to hit a sphere of the molecule, it is equal to the  $y$  initial position of the particle or  $y \pm R$  depending on its initial position, it can range from  $-(R + \sigma/2)$  to  $(R + \sigma/2)$ .

For each impact of a particle against the molecule the particle changes its total momentum and such variation is equal to the impulse of the force that the molecule exerts on the particle in the time interval in which the contact molecule-particle happens. Let us indicate with  $\delta t$  the aforementioned time interval and with  $F$  the average force which the molecule exerts on the par-

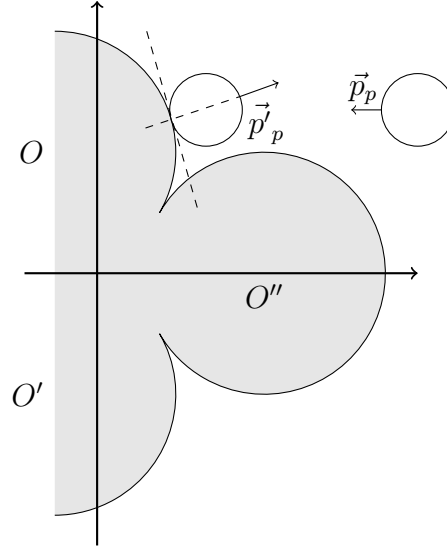


Figure 3.2: In this image we want to represent how the collision between the particles and the molecule happens. A particle arrives from  $\pm\infty$  carrying a momentum only in the  $x$  direction, it collides with the molecule and it bounces off elastically in the direction perpendicular to the surface of the sphere in that point. The absolute value of the momentum doesn't change and remain constant. The particles are evenly distributed along  $y$  in the interval  $[-(2R + \sigma/2); (2R + \sigma/2)]$ .

ticle, the impulse is thus  $F\delta t$ . For Newton's third law the average force that the particle exerts on the impact against the molecule is therefore

$$\vec{F}\delta t = -\Delta\vec{p}_p. \quad (3.0.3)$$

Let us integrate both members of the equation on time

$$\int_0^\tau \vec{F}\delta t dt = \int_0^\tau -\Delta\vec{p}_p dt, \quad (3.0.4)$$

where  $\tau$  is a time interval long enough that every interval along the  $y$  direction get visited. Afterwards we can exchange the integral on the time with a integral on the spacial coordinate  $dy$  and we obtain

$$\int_0^\tau \vec{F}\delta t dt = \int_{\text{all possible } y} -\Delta\vec{p}_p dy = -p_p \int_{\text{all possible } y} (\pm \cos \phi \hat{\mathbf{i}} \pm \sin \phi \hat{\mathbf{j}} \pm \hat{\mathbf{i}}) dy, \quad (3.0.5)$$

where again the plus and minus signs depends on the initial position of the particle considered. We can drop the last term, since the integral on all the possible  $y$ , in the two direction of a constant is null.

For simplicity we will now split the calculation between the resultant of the right part of the molecule,  $\vec{F}_{right}$ , the one that gets hit by spheres with negative momentum, and the resultant of left part,  $\vec{F}_{left}$ . We obtain

$$\vec{F}_{right} = \sum_{O, O', O''} -p_p \int [\cos \phi \hat{i} + \sin \phi \hat{j}] dh. \quad (3.0.6)$$

Knowing the inverse trigonometric functions

$$\cos(\arctan x) = \frac{1}{\sqrt{1+x^2}} \quad \text{and} \quad \sin(\arctan x) = \frac{x}{\sqrt{1+x^2}}, \quad (3.0.7)$$

we get that

$$\cos(\arctan \phi(h)) = \frac{1}{\sqrt{1 + \frac{h^2}{(R+\frac{\sigma}{2})^2 - h^2}}} = \frac{\sqrt{(R+\frac{\sigma}{2})^2 - h^2}}{R + \frac{\sigma}{2}} \quad (3.0.8)$$

and

$$\sin(\arctan \phi(h)) = \frac{h}{\sqrt{(R+\frac{\sigma}{2})^2 - h^2}} \frac{1}{\sqrt{1 + \frac{h^2}{(R+\frac{\sigma}{2})^2 - h^2}}} = \frac{h}{R + \frac{\sigma}{2}}. \quad (3.0.9)$$

The  $y$  component of the momentum is odd and the sum of the intervals of integration is even, so the  $y$  component is null.

Let us name  $R + \sigma/2$  as  $k$  for clarity and therefore we obtain

$$F_O|_x = -p_p \int_{-k}^k \cos \phi dh = -p_p \int_{-k}^k \frac{\sqrt{k^2 - h^2}}{k} dh = -p_p \int_{-k}^k \frac{\sqrt{1 - \frac{h^2}{k^2}}}{k} dh. \quad (3.0.10)$$

Using the substitution

$$x = \frac{h}{k},$$

we get

$$F_O|_x = -p_p \int_{-1}^1 \sqrt{1-x^2} k \, dx. \quad (3.0.11)$$

As we know if we put  $x = \sin t$

$$\begin{aligned} \int \sqrt{1-x^2} \, dx &= \int \sqrt{1-\sin^2 t} \cos t \, dt = \int \cos^2 t \, dt = \frac{t}{2} + \frac{\sin 2t}{4} + c \\ &= \frac{\arcsin x}{2} + \frac{1}{2} \sin(\arcsin(x)) \cos(\arcsin(x)) + c \\ &= \frac{\arcsin x}{2} + \frac{1}{2} x \sqrt{1-x^2} + c. \end{aligned} \quad (3.0.12)$$

Thus

$$F_O|_x = -\frac{kp_p}{2} \left[ \arcsin x + x \sqrt{1-x^2} \right]_{-1}^1 = -\frac{kp_p}{2} \pi. \quad (3.0.13)$$

Similar calculations bring us the result for the other two integrals.

$$\begin{aligned} F_{O'}|_x = F_{O''}|_x &= -\frac{kp_p}{2} \left[ \arcsin x + x \sqrt{1-x^2} \right]_{\frac{\sigma}{2k}}^1 \\ &= -\frac{kp_p}{2} \left[ \left( \frac{\pi}{2} - \arcsin \left( \frac{\sigma}{2k} \right) - \frac{\sigma}{2k} \sqrt{1 - \frac{\sigma}{2k}} \right) \right]. \end{aligned} \quad (3.0.14)$$

So we get

$$F_{right}|_x = -kp_p \left( \pi - \arcsin \left( \frac{\sigma}{2k} \right) - \frac{\sigma}{2k} \sqrt{1 - \frac{\sigma}{2k}} \right). \quad (3.0.15)$$

We can now calculate  $F_{left}$  as the integral on the two spheres, with the right interval of integration. The consideration we did before are still valid now and the  $y$  component is null here too. In addition we have that the integral on the  $x$  component of  $O'$  is equal to the one on  $O$ .

$$\begin{aligned} F_{O'}|_x = F_{O''}|_x &= p_p \int_{-R}^k \cos(\phi) \, dh = p_p \int_{-R}^k \sqrt{1 - \frac{h^2}{k^2}} \, dh = kp_p \int_{-\frac{R}{k}}^1 \sqrt{1-x^2} \, dx \\ &= \frac{kp_p}{2} \left[ \frac{\pi}{2} + \arcsin \left( \frac{R}{k} \right) + \frac{R}{k} \sqrt{1 - \frac{R^2}{k^2}} \right] \end{aligned} \quad (3.0.16)$$

So  $F_{left}$  is equal to two times the result in equ. (3.0.16).  
Finally we obtain the total momentum as

$$\begin{aligned}
 F_{Tot}|_x &= F_{Left}|_x + F_{Right}|_x \\
 &= kp_p \left[ \frac{\pi}{2} + \arcsin\left(\frac{R}{k}\right) + \frac{R}{k} \sqrt{1 - \frac{R^2}{k^2}} - \pi + \right. \\
 &\quad \left. + \arcsin\left(\frac{\sigma}{2k}\right) + \frac{\sigma}{2R + \sigma} \sqrt{1 - \frac{\sigma}{2R + \sigma}} \right] \\
 &= kp_p \left[ -\frac{\pi}{2} + \frac{R}{k} \sqrt{1 - \frac{R^2}{k^2}} + \arcsin\left(\frac{\sigma}{2k}\right) + \frac{\sigma}{2k} \sqrt{1 - \frac{\sigma}{2k}} \right]. \quad (3.0.17)
 \end{aligned}$$

We can see that there is a force different from zero on the  $X$  axis acting on the molecule if we get a time interval long enough, in this configuration. Since the molecule is symmetric over the  $X$  axis we expected no force at all along the  $Y$  axis, and so it is. We can see in Fig. 3.3 the trend of the force in function of  $\sigma$ .

Let's keep our attention on the  $X$  axis from now on and let us imagine that the molecule is free to move only in the  $X$  axis direction, as if it had an ideal constraint. If we now consider two changes of coordinates of the  $X - Y$  axis and of the set up, of a rotation of  $120^\circ$  and  $240^\circ$  we get that the  $X'$  and  $X''$  axis pass through the centre of the  $O'$  and  $O''$  spheres respectively.

We keep the particle fixed on the old  $X$  axis rails, but let us consider the collision with the particles coming also along the new  $X'$  and  $X''$  axis carrying momentum only in the  $X'$  and  $X''$  direction, uniformly distributed along the  $Y'$  and  $Y''$  axis respectively. What we would obtain if the molecule was not on tracks and hit only in the  $X'$  or  $X''$  direction would be a drift along the corresponding axis in accordance with the results above. Instead since the molecule can move only in a fixed direction, and we receive particles from the three directions the particles in the other direction gives us a contribute of  $-P_{x'}/2 - \sqrt{3}P_{y'}/2$  and  $-P_{x''}/2 + \sqrt{3}P_{y''}/2$

In the second part we want to uncover how the fluctuations on the moment distribution of the molecule struck in the three directions behave, because the simple sum of all the elements we considered would give us a still molecule in average, while the fluctuations under some condition can bring us a different result.

We can see in Fig. 3.5 the pattern of the exchanged momentum in function of the three impact parameters  $y$ ,  $y'$  e  $y''$ . The functions concerned are not reversible and we could not get the distribution of the momentum analytically, but since the functions are continuous, except for a few numerable

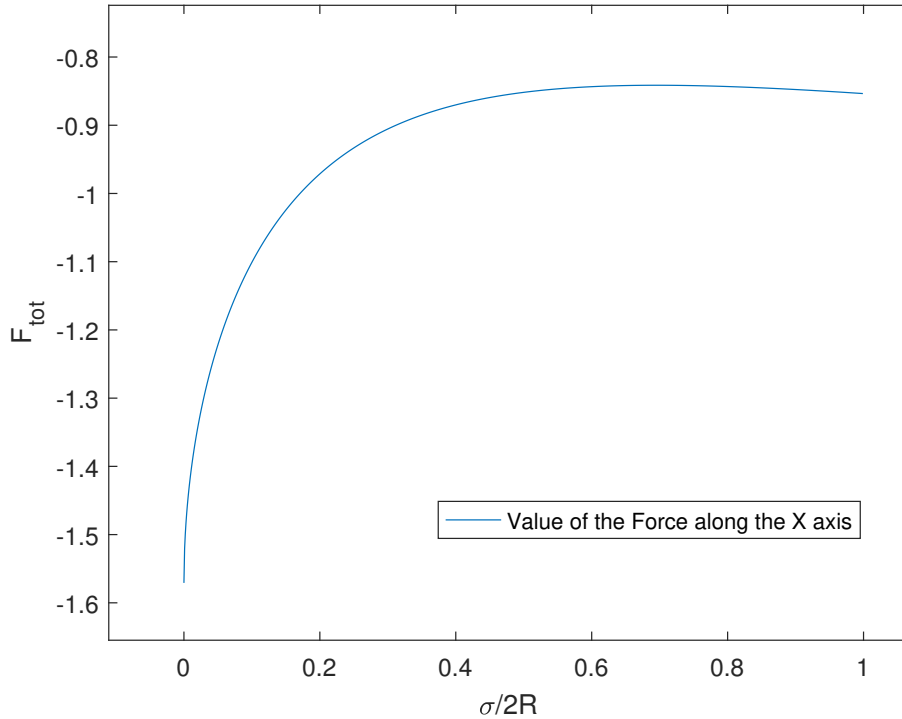


Figure 3.3: This image shows the value of the total momentum along the  $X$  axis in function of  $\sigma/2R$

discontinuous points, we obtained it computationally through a simple program in which for every step of the impact parameter we calculated a value of the function with which we built an histogram out of all the values. In Fig. 3.6 we can see some examples at different values of  $\sigma/2R$ .

Afterwards we calculated the median value and the average value of the histogram thus created and in Tab. 3.1 some of the results are shown.

In a stationary situation, in which there is no gradient in temperature, the particle won't change its position, in average, while if there is one, the fluctuations on the momentum give us information if there is the possibility of a drift.

As expected, when  $\sigma$  is null the distribution of the values is symmetrical and the median and the average are equal to zero too. When the value of  $\sigma$  is different from zero the symmetry is broken and the median is negative while the average is still compatible to zero due to the error caused by the computation approximations. As sigma grows, as we can see in the Fig. 3.6 the imbalance between the left and the right part is more evident, but the

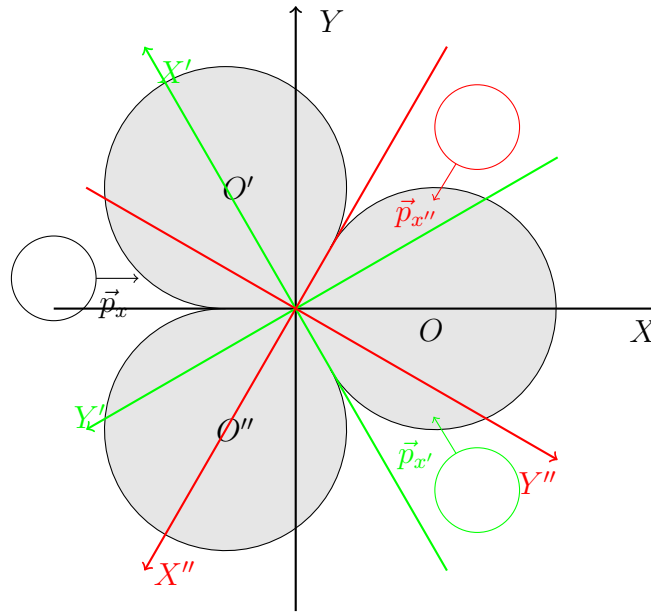


Figure 3.4: In this figure we show the two change of coordinates considered. The  $X' - Y'$  coordinates (in green in the figure) are obtained rotating the  $X - Y$  axis of an angle of  $2\pi/3$ , while the  $X'' - Y''$  coordinates (in red in the figure) are obtained through a rotation of  $4\pi/3$  in respect of the  $X - Y$  axis. Particles can arrive from the three directions carrying momentum only in the direction from which they arrive.

median reach a sort of threshold. The null average is compatible with the results obtained in the first half, if the molecule is hit by the particles in the three direction equally distributed along the three impact parameters the molecule will in average stay still. Instead if there is a gradient of temperature, since the median is not null, the fluctuations of values of the exchanged momentum can let the molecule experience a drift.

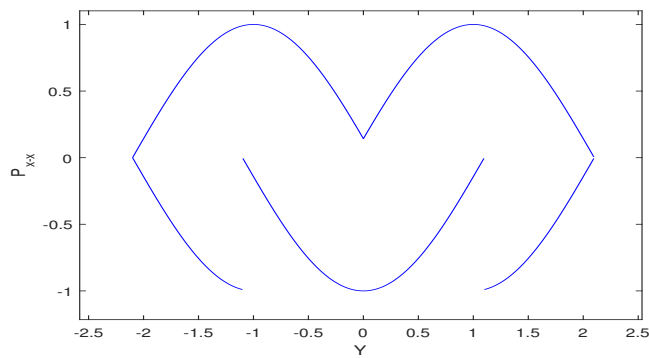
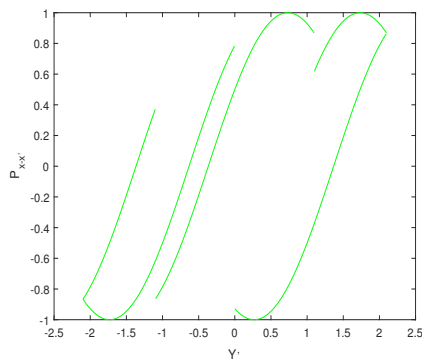
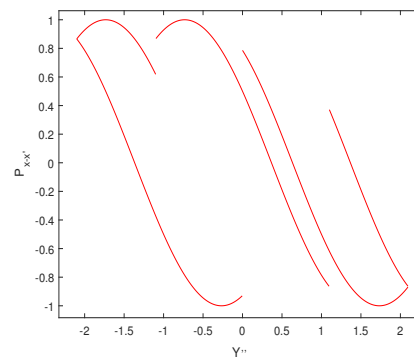
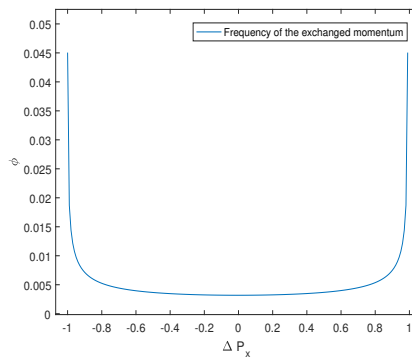
(a) The system of the  $X - Y$  coordinates(b) The system of the  $X' - Y'$  coordinates(c) The system of the  $X'' - Y''$  coordinates

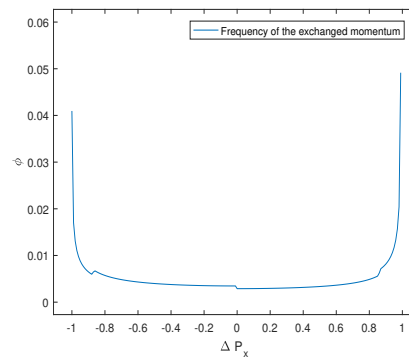
Figure 3.5: Value of the exchanged momentum, along the x-axis, in function of the impact parameter, respectively  $y$ ,  $y'$  e  $y''$ . For obtaining these images we used as values  $R = 1$ ,  $\sigma/2 = 0.1$  and  $p_p = 1$ .

$\frac{\sigma}{2R}$	Median	Average
0	$1.1 \times 10^{-16}$	0
0.2	-0.03	$6.7 \times 10^{-5}$
0.4	-0.06	$1.3 \times 10^{-4}$
0.6	-0.07	$1.4 \times 10^{-4}$
0.8	-0.07	$1.5 \times 10^{-4}$
1	-0.07	$1.5 \times 10^{-4}$

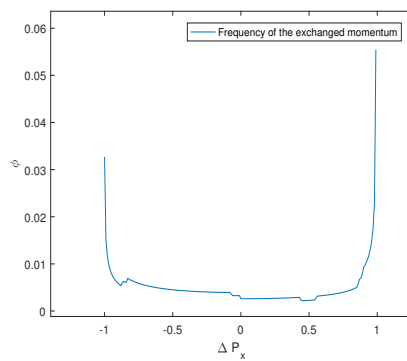
Table 3.1: The value of the median and of the average of the distribution of the momentum, in function of  $\sigma/2R$



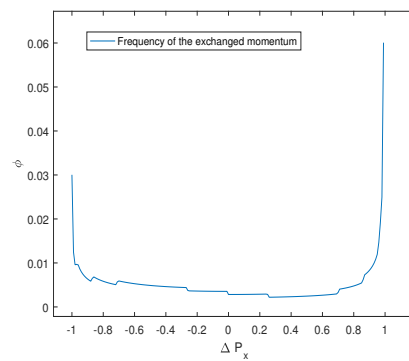
(a)  $\sigma/2R = 0$



(b)  $\sigma/2R = 0.2$



(c)  $\sigma/2R = 0.6$



(d)  $\sigma/2R = 1$

Figure 3.6: In these images are shown the distribution of the value of the momentum exchanged at different values of  $\sigma$

# Chapter 4

## Program and Simulations

In this thesis project I used the program developed by dr. Matteo Monti and dr. Carlo Emilio Montanari called *Not Only Colliding Spheres* (NOCS) written in the programming language C++. The program is still under development and in this thesis project we have tested some of its key elements.

We want now to give to the reader an idea of how the program works and if someone is interested in this topic it is possible to have more information following the link mentioned in the bibliography [7].

### 4.1 Not Only Colliding Spheres

NOCS has been important to study and understand how the effects of excluded volume works with spheres and Boltzmann gases. In fact all of its features and its capability to adjust to the many situation which have emerged in our study make it one extremely useful tool on this topic.

NOCS is an exact event driven program developed for the simulation of motion of molecules in two dimensions with periodic boundary conditions.

Furthermore if the user needs some particular data, or conditions, for his simulation, it is possible to implement two kinds of lambda expressions that will help the user to reach the goal of his simulation.

Let's see some of the most important features of the program NOCS through the highlighting of its most important classes and lambda expressions.

#### **The class Engine**

The class Engine is the core of the entire simulation, because it takes care of the actual execution of the processes simulated. The Engine stores the objects of the simulation and it builds a queue of event objects.

The fact that the program is event based means that the time evolution doesn't happen as in a normal simulation of motion, where all particles evolve over time at the same time. Instead a queue of events is created and only when an event, like a bump between molecules, happens the position of the particles involved are changed. It is like to keep all the particles not involved in an event backward in time until they actually are involved in a event and then to change their positions, their equations of motion and that of the other particles that may interact with them, and to build afterwards a new queue of events.

While it may seem unnatural to use such a simulation method, it is important for cutting down computational time considering that in models with many body, simulations with exact dynamics are too time consuming. While other methods may be employed, like the use of Monte Carlo simulation, a program able to develop exact dynamics in an acceptable time is extremely enticing.

The queue of events is obtained through the equation of motion of all the particles, bumps happen elastically, along the line joining the centre of mass of the two particles and the total energy and the total momentum are conserved. Particles also can carry an internal momentum and are able to rotate.

The class Engine works with a decided by the user amount of time, meaning that it must develop the queue of events until the decided time. After the decided time the position and the momentum of all the particles are upgraded to what they should be if a normal dynamic was happening, through integration of the equations of motion. Afterwards another time interval may be given to the class Engine that makes the procedure start again from the newly calculated positions and momenta.

This feature is useful if in a particular simulation for example is needed to know how the position of some particle evolves. It is still important to not give a set of time intervals too small because the integration of the equation of motion gives an intrinsic computational error, and also because it would be too costly in computational time, making the implementation of a event driven program useless.

The class Engine also provides a subscription system that allows the user to observe only the desired events of the simulation, so to gather only the required data without wasting computational time.

### **The class Grid**

The class Grid implements a subdivision of the simulation zone into smaller squared regions, when the engine is established the finesse of the grid must

be set.

The space where the simulations of NOCS happens is a square with an edge of length one, but since the dimension of the molecule considered must be quite smaller it is unpractical to build a queue of events comparing each element of the simulation with each other, since it would require a great deal of computational time. The subdivision in smaller squares reduce the volume of many analysis, in fact after the subdivision happens each element of the simulation needs now to be compared only with the other elements in their region and in the neighbouring regions.

It is important to impose a grid with cell bigger than the particles present in that particular simulation, or the simulation may work poorly, but as small as possible, for reducing the computational cost.

### **The class Molecule**

The class Molecule is the object-oriented representation of a generic molecule of arbitrary shape and mass in dynamic motion, inside a 2-dimensional space.

A molecule is built up totally by the user as it is more fit for his uses in a particular simulation.

The user may set properties that gives the molecules their characteristic: the relative position of the spheres which compose the molecule (with the condition that they must overlap, or at least they must be tangent to each other), the mass, the radius of the spheres, the relative position of the centre of mass. Also the external proprieties that dictate the interaction with the other particles must be set, like the position and the velocity of the centre of mass, the orientation and the angular velocity.

When a molecule is inserted in the engine it receives an id from the program that identifies it, in addition the user may give one or more tags to a molecule, thanks to the class Tag.

### **The class Tag**

The class Tag is a public nested class of the class Engine, this class is what allows to identify any object of the simulation with a series of system-defined and user-defined tags.

In fact when an object like molecule gets implemented is possible to include the class Tag. Doing so will give to the chosen molecule a label chosen by the user that will permit to the program to differentiate between molecules, or group of molecules, with different tags.

Since often the user is interested on how the properties of some particular molecule evolves or change, this feature is extremely helpful in doing so.

To any molecule, or group of molecules, any number of tags may be added.

### **The class Bumper**

The class Bumper is an object-oriented representation of a spherical immovable obstacle in a two dimensional space. When a bumper is implemented together with the position and the dimension of the bumper itself a tag can be added.

### **The class Event**

The class Event is the abstract base class for the engine's event system. It may represent the collision of a molecule with a bumper, a molecule against a molecule or a molecule changing region inside the grid of the engine. This guarantees space continuity by performing translations on the molecules when it is required.

### **The classes Resetter and Elasticity**

The class Resetter is a component of Engine which allows the user to set the value of energy of a molecule, or a group of molecules, with a chosen tag, into any desired value, maintaining all the internal proportions between them (translational and rotational).

The class Elasticity enable the user to set certain events (impact between certain tagged molecules or between certain molecules and bumpers) as anelastic (in the impact some of the energy get dissipated) or superelastic (in the impact the energy get increased).

These class are useful when we want to study effects taking place at the imbalance, or when we want to simulate a transition of energy between a hot and a cold spot, for example.

### **The lambda expression Engine.on**

The lambda expression Engine.on permits to the user to write expressions that will be inserted in the queue of events, once a determined event that triggers the effect of Engine.on happens in the simulation. The lambda expression Engine.on offers the most versatile uses and it is the most useful tool in NOCS.

### The lambda expression Engine.each

The lambda expression Engine.each permits, at a given time, to get all the possible information needed by the user on a particular set of molecules with the same tag. In addition this expression can repetitively perform a task for all the molecules in the chosen set.

### Graphics

NOCS offer also the opportunity to visualise the two dimensional simulation while it happens. While it is not recommended to use the visualising through a long simulation, due to its computational cost, it is useful during trials for understanding if the system simulated is meaningful.

## 4.2 Effects of the Excluded Volume

We want now to disclose to the reader the results of the simulation done for this thesis project. In this section we present the simulations, obtained through NOCS, of a system, a gas, of two kind of spherical particles, bigger colloidal-like particles and smaller ones, which act as depletants. We want to answered to two issues, firstly how the potential behaves. This is a topic often found in literature [6] and we tried to follow the examples of

Secondly we want to estimate the time of clustering for the bigger particles. This is important in many systems, in fact for many chemical or biological reaction to take place is needed an activation time, and to understand if and how the effects of the excluded volumes have played a role in the formation and in the shaping of the proteins would be interesting.

The simulations are in function of two parameters

- The *ratio between the radii* of the two different particles present in our gas,
- The *occupancy*, which is the occupied area by all the particles divided by the total area of the box.

It is important to choose an appropriate occupancy, because a system with an occupancy too big may cause effect of jamming, that is a phase transition, in which a local event may have an impact on all the system. It can describe some physical process like glasses, foams or emulsions but we are not interested in treating these topics in this projects. Instead the simulation of a too rarefied gas would not let us understand how the excluded forces relate with the thermal noise of a Boltzmann gas, not helping us to understand the dynamics of the molecules in a true gas.

### 4.2.1 Determination of the Potential

For figuring out the shape of the potential we did two kind of simulation

#### Estimation of the Exchanged momentum

As we described in the third chapter, between two spheres at a fixed distance surrounded by smaller spheres which act as depletants act a force, when the distance between the two bigger spheres is compatible with the diameter of the smaller spheres, as an effect of the excluded volume. And if given enough time, the exchanged momentum may be considered a force.

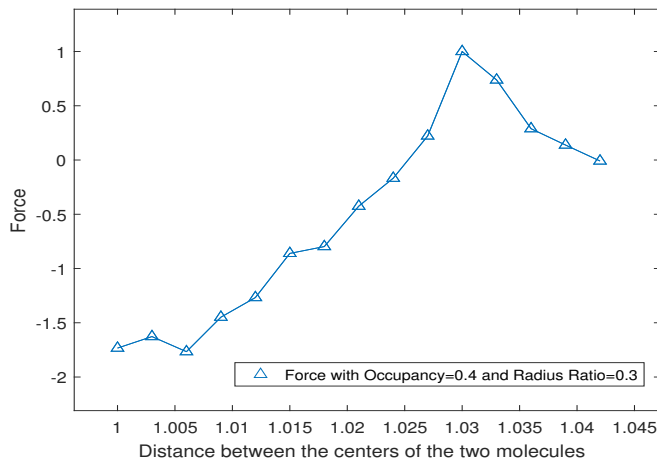
In the first simulation done we placed two particles at a fixed distance  $h$  giving them a considerable mass, bigger then ten order of magnitude than the other particles, and no kinetic energy at all, this way we could consider the two spheres fixed at the given place for a reasonable time intervals.

This simulation can't be considered truly dynamical because the element of concern, the potential, is obtained blocking the bigger spheres for a time which can be considered infinite. The potential thus found may not have an actual effect when all particles are free to move because the thermal noise of the gas could cover up the effect of the potential.

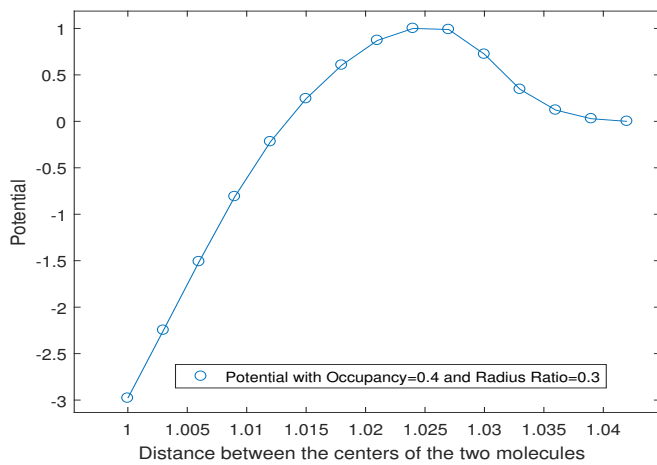
The two bigger spheres are placed at the centre of the square in which our simulation happens and the radii of the two bigger spheres are chosen to be the 0.05 of the aforementioned square. The centres are placed at the same  $y$  coordinate, at the same height.

The smaller particles are able to move freely in the two dimensional squared box with periodic boundary conditions, have a small mass compared to the bigger spheres and at the beginning of our simulation are given a fixed position each and a kinetic energy distributed according to a normal distribution and an initial random direction of motion. The radius of the smaller spheres is given in function of that of the bigger spheres, it can vary from the 0.25 to the 0.35 of the aforementioned radius of the bigger spheres. The number of the smaller spheres are decided by the occupancy, the quantity of total area covered by all the particles.

After an initial time of mixing we can consider our system to have achieved an equilibrium and then we start to collect the exchanged momentum at the impact between the smaller spheres and the two bigger spheres. We want to obtain the total exchanged momentum along the axis passing through the centre of the two spheres, since the shape of our configuration has an effect only along the aforementioned axis. As we explained in the third chapter, if given enough time the sum of all the momenta is like a force acting between the two bigger particles. We project the exchanged momentum of each bigger



(a) In this figure we can see the profile of the force obtained through this simulation in function of the distance. Each point of the force was obtained blocking the position of the two molecules at the needed distance, and letting the system exchange momentum with the particle and as seen in the third chapter if enough time was given the sum of all the exchanged momentum can be considered a force.



(b) In this figure we can see the profile of the potential acting between the two molecules in function of the distance between them. This profile is obtained through numerical integration of the previous force profile and shift of the value along the y-axis so to have zero has value of the last point. This was done because after a diameter and half of the smaller spheres the effect of the entropic force is not relevant, and the value oscillates around the zero.

particle on the axis of interest and sum all of it up to obtain a relative value of the force acting at the fixed distance  $h$ , between the two bigger particles.

We repeated the process at different values of  $h$ , keeping all the other variables constant, the number of the time steps included, we repeated the same simulation for five times and averaging the results thus obtained we arrive at a profile for the force, as we can see in Fig. 4.1a for the case with occupancy equal to 0.4 of the total area and a radius ratio of 0.3.

Once we obtained the profile of the force, we have integrated it numerically, thus achieving the shape of the potential acting between the two bigger spheres as shown in Fig. 4.1b.

We can see in Fig.4.2 a comparison between the profiles of the potential obtained by varying the occupancy and by keeping the radius ratio constant. As we can see as the occupancy increases the depth of the potential well increases as well. For the case of Occupancy 0.5 we can see a second well of potential, typical of the entropic forces at such concentrations of particles, as presented in the paper [8].

Secondly in Fig. 4.3 is shown comparison of the profiles of the potential obtained by varying the radius ratio and by keeping the occupancy constant. As we can see the depth of the potential well doesn't change much in this range of variation of the radius ratio. It is shown that the potential generated by the smaller spheres of different dimension have a different range of action. In fact the length of the potential well is determined by the length of the diameter of the smaller spheres which act as depletants.

In Fig. (4.4) we show the comparison between the theoretical profile of the potential as obtained in the second chapter in equ. 2.1.6, and one of the simulation done at occupancy 0.4 and at radius ratio 0.3. The trend of the potential obtained through the simulation is a good approximation, except when the two molecules get further away then the diameter of the smaller spheres.

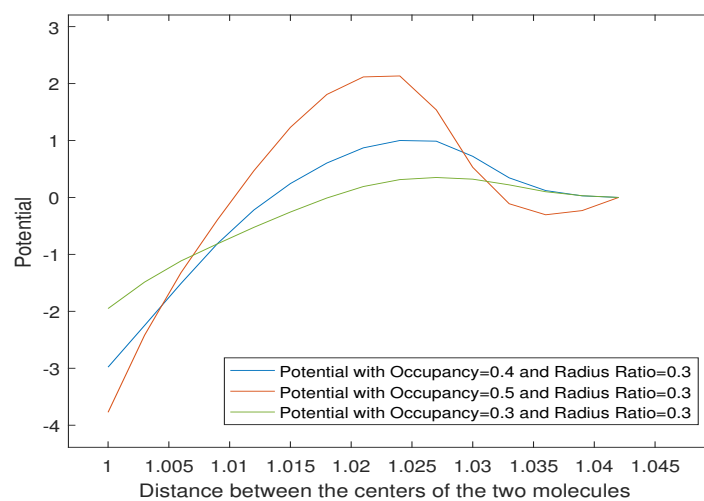


Figure 4.2: In this image are shown all the potential obtained by varying the occupancy, while maintaining constant the radius ratio. We can see that as the occupancy increases the depth of the potential well increases as well.

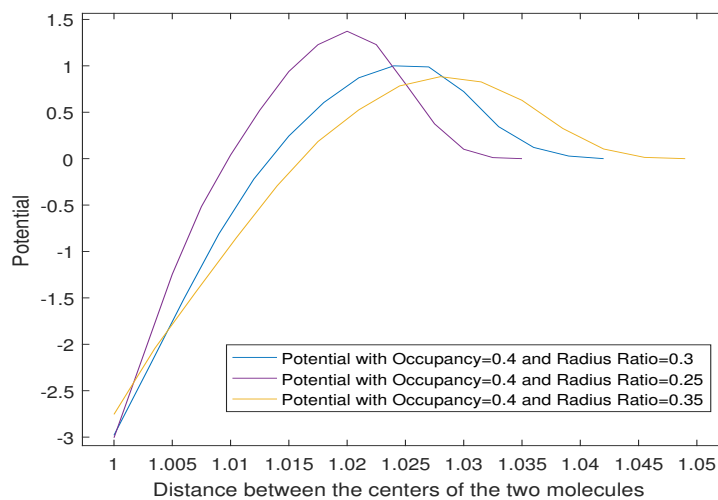


Figure 4.3: In this image are shown all the potential obtained by varying the radius ratio, while maintaining constant the occupancy. We can see that as the radius ratio diminishes the potential well, but only a little. We can also see that the potential generated by the depletants of different dimension have a different range of action. In fact the length of the potential well is determined by the length of the diameter of the depletants.

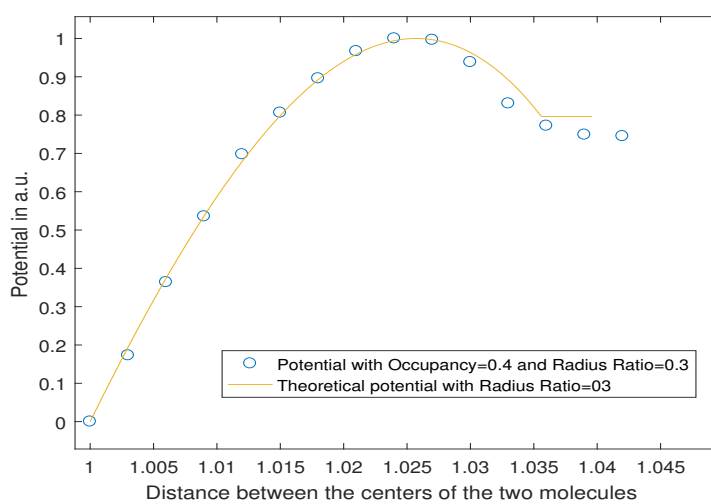


Figure 4.4: In this figure it is shown in blue circles the potential in function of the distances between the centre of the molecules at radius ratio 0.3 and occupancy 0.4, in orange is shown the profile of the theoretical potential obtained in the second chapter in equ. 2.1.6 in arbitrary units.

### Estimation of the Distribution of the Distances

The other method we followed for computing the potential is a dynamic method. In this simulation all the particles can move freely.

We know that in gas, when is present a potential between particles, the distribution of the positions follows the Maxwell-Boltzmann distribution

$$P(N, x) = A e^{-\frac{W(x)}{kT}}, \quad (4.2.1)$$

where  $P$  is the probability to have the two particle be at a distance  $x$ ,  $N$  is the number of particle present,  $A$  is a normalisation constant,  $k$  is the Boltzmann constant,  $T$  is the temperature of the system and  $W$  is the potential existing between the particles.

We want to obtain the potential through a measure of the distribution of the distances. The distances obtained in the system simulated with NOCS will be compared to a null model which will be built for differentiate between the effect of the potential and the statistical effects.

In fact we have that:

$$P_0(N, x) = A_0 e^{-\frac{W_0}{kT_0}}, \quad (4.2.2)$$

where  $P_0$  is the probability to have two particles at the distance  $x$  for a gas without potential acting between,  $N$  is the number of particle present,  $A_0$  is a normalisation constant,  $W_0$  is a constant potential,  $k$  is the Boltzmann constant and  $T_0$  is the temperature of the system.

From the equations (4.2.1) and (4.2.2) we have

$$\frac{P(N, x)}{P_0(N, x)} = \frac{A}{A_0} e^{-\frac{W(x)kT_0}{W_0kT}}, \quad (4.2.3)$$

and making the logarithm of the previous equation we obtain

$$\log \left( \frac{P(N, x)}{P_0(N, x)} \right) = -\log \left( \frac{A}{A_0} \right) \frac{T_0}{W_0 T} W(x), \quad (4.2.4a)$$

$$W(x) = -B \log \left( \frac{P(N, x)}{P_0(N, x)} \right), \quad (4.2.4b)$$

where  $B = \frac{W_0 T}{T_0 \log \left( \frac{A}{A_0} \right)}$  is a constant, since the temperatures are arbitrary and in our simulations and they remain constant.

For calculating the effects of the potential we introduced a set of ten bigger spheres labelled as *Big*, trough the class `Tag` of NOCS, the radius of the bigger spheres are chosen to be the 0.05 of the edge of the square where the simulation happens. The bigger spheres are positioned at the beginning

of the simulation on the lower part of the square and are given a kinetic energy distributed according to a normal distribution a finite mass and an initial random direction of motion.

It is not so important the attribution of a certain energy or mass to the bigger spheres, what is important is the ratios of the energy and of the masses between the bigger and the smaller spheres.

We attributed to the smaller particles a mass related to the bigger spheres through the ratio of their area, we have chosen to give the same density to both particles. We gave them the same value of kinetic energy of the bigger spheres, for the normal distribution, so they are less massive, but faster, since we consider the gas to be at the same temperature. Again the number of the smaller spheres are decided by the occupancy, the quantity of total area available to be covered after we subtracted the area covered by the bigger spheres.

After an initial time of mixing we reach a stable configuration and we begin our measurements.

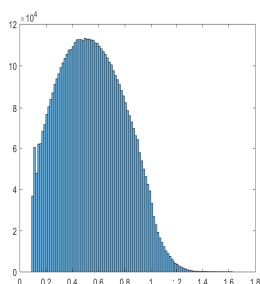
We want to obtain the distribution of the relative distances between all the closest *Big* spheres, so using the lambda expression Engine.each, after a chosen time interval, we got the positions of every particle and we calculated the matrix off all the distances. Afterwards we selected, to add to our data, only the closest particle for each particle. We built the program so that the chosen time interval was sufficient to let the particles mix and have independent measurements of the positions. We used all the relative distances to build a histogram in function of the distances. Afterwards we built a distribution of all the distances thus obtained, as we can see in Fig. 4.5a.

For the construction of the null model, we decided to use a Monte Carlo experiment. We let the program distribute some points, in a two dimensional box, in a random fashion. We placed as many points as the number of particles of the dynamic experiment explained before.

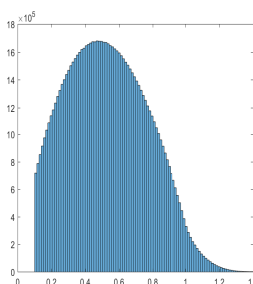
We imposed an acceptance condition on the random placement, which is that two centres of all the particles considered cannot be closer to each other than a length equal to the diameter of the spheres. The acceptance condition is used to represent the impossibility of overlapping for two particles.

The ratio of the acceptance parameter with the edge of the squared box where the points are placed is 0.1, the same ratio of the diameter of a *Big* particle with the square of the previous experiment.

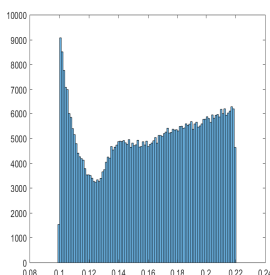
Again we are interested in the distribution of the relative positions, so after taking all the position at a fixed frame in the simulation we build a matrix with all the distances, and afterwards we let the program evolve. We let all the points, one at a time while all the other points are fixed,



(a) In this figure we can see the histogram with the distribution of the distance between the centres of the molecules, of the other closest molecule to each molecule in our simulation.



(b) Here we show the distribution of the distances of the null model build through a Monte Carlo simulation, again we don't have any molecule closer to each other of a diameter of a molecule. The shape of the distribution is that of a truncated gaussian.



(c) In this image we show a magnification of the histogram shown in the figure (a), with a focus on the distances covered by the range of the potential.

choose a new acceptable random position. We repeat the procedure for 1000 times and then take a new frame, this way we can consider, at every frame used for calculating the distances, the positions to be independent from the previous positions and we thus obtain the distribution. As we can see from Fig. 4.6 the shape of the potential thus obtained is almost equal to the shape obtained through the previous simulation. The only difference between the two potentials is in the sharper decay of the peak in the second simulation. This is due to the fact that in the first simulation the molecules were blocked at all the distances for an equal amount of time, while in a true dynamical simulation we think that the molecules in average spend less time in that

range, so the value is diminished after the peak.

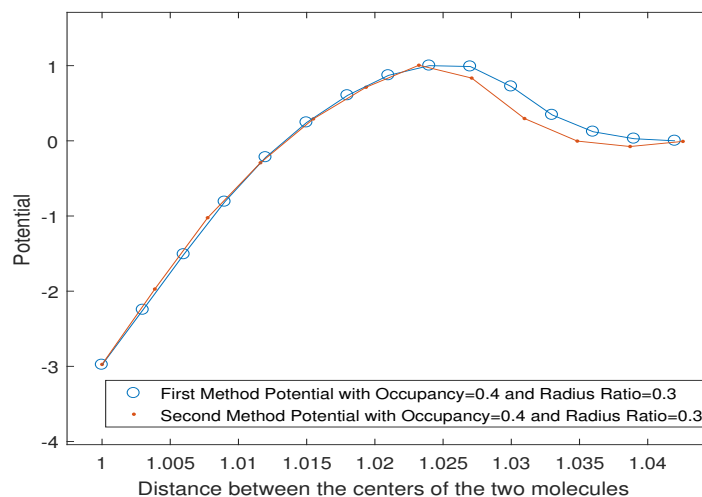


Figure 4.6: In this figure it is shown in red the potential in function of the distances between the centre of the molecules, obtained through the process just explained, in blue we can see in comparison the shape of the potential obtained in the first kind of simulation. The red profile of the potential was obtained through a dynamical simulation. Both profile are obtained with an occupancy of 0.4 and a radius ratio of 0.3. Both profiles are normalised to the height of the highest peak.

## 4.2.2 Estimation of the Clustering Time

One of the main reason we started this project was to understand and quantify how the particles stay close to each other. This is important because in nature many events, like chemical or biological reactions need time to let them happen.

We wanted, through a simulation, to measure how the time intervals in which the molecules spend time close to each other varies.

We used the same computational set up of the last experiment, we introduced a set of 10 molecules, labelled as big, free to move in a two dimensional box and a higher number of smaller particles which act as depletants, in dependence to the parameter occupancy, which decided how much of the total space is occupied.

After an initial time of mixing of the system, needed for reaching a stationary condition, we started to measure how much time two particles spend close to each other.

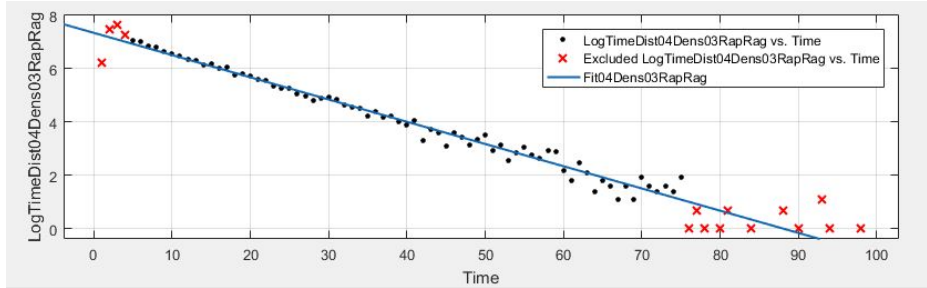


Figure 4.7: We show how the data for the fits are selected. We chose to exclude the data when the semi-log distribution starts to go often to zero and when there in the initial bulk. Increasing the simulation time may help to get a better result but it isn't necessary to our purpose.

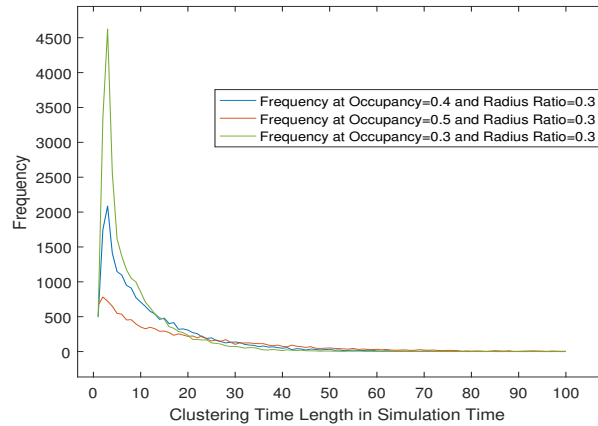
As we can see in the Tables 4.1 and 4.2 the Slope of the lines obtained decrease, in absolute value, as the occupancy grows and as the radius ratio grows.

After two particles got closer than the first threshold, we started to count how many time steps they spent together and after the molecules move further away than a second threshold we stopped the count and added one to the appropriate cell of the array used to record the time intervals, this way we could obtain the distribution of how often a certain time interval would occur, given the radius ratio and the occupancy.

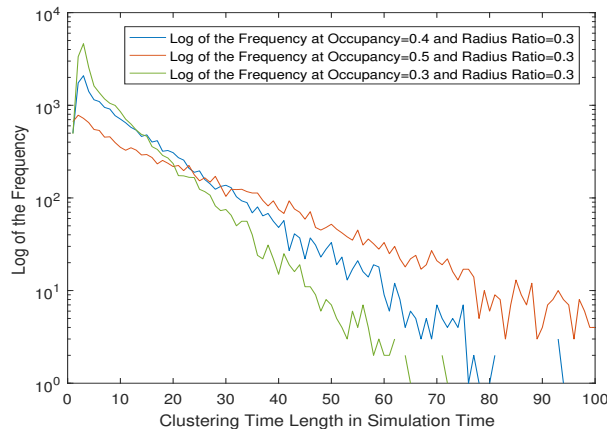
We chose to apply two different threshold because otherwise the low value of time interval would be overestimated. We choose to use as first threshold between the distance of the centre of the bigger molecules a diameter of the two molecules plus 1.5 times the radius of the depletant particles. This because the range of the force acting between the molecules due to the depletant is at maximum two times the radius of the depletant, but since some particles may arrive with a strong kinetic energy they may not perceive the potential well if they do not get close enough to each other.

After some trials, we saw that if we used the same threshold for when the particles moved away from each other we got an extremely high value for small time interval, we thought that the molecules might fluctuate near the threshold and thus we overestimated the small time intervals. Instead after using a second threshold of two times the radius of the smaller depletants, the effect previously described was greatly reduced.

We can see in Fig. 4.8a as the trend of the distribution change in function of the occupancy and in Fig. 4.9a the changes in function of the radius ratio. We show also the semi-log graph in Fig. 4.8b and 4.9b, for better understanding.



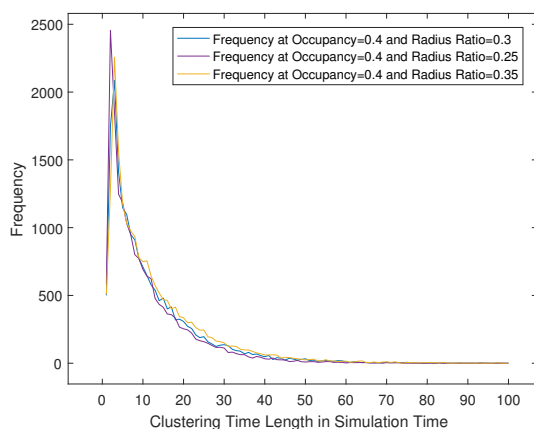
(a) In this image are shown the distributions of how much time two particles are close together. The distributions are in function of the occupancy and of the radius ratio. Every value of the time length corresponds to 0.15 seconds of simulation time. In this image we show three of the distribution obtained varying only the occupancy. We can see a clear negative exponential behaviour.



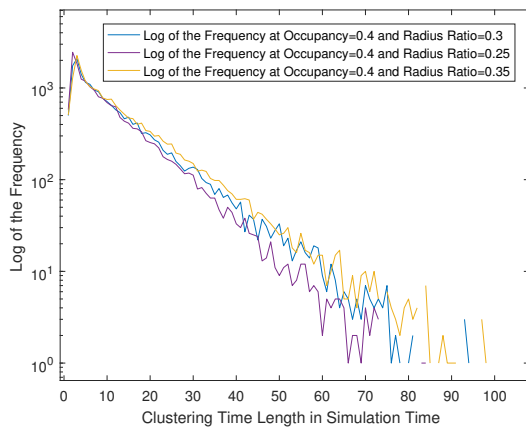
(b) The distribution shown in (b) are the logarithmic scale of the distribution in the previous image, we can see that as the occupied area increases (from green to blue to red) the time that the particle tend to stand close to each other increases too.

Figure 4.8

We can see a big number of small time interval, probably caused by the fact that when two particle spend time close to each other and get apart they may get close together again, oscillating and thus overestimating the smaller time intervals. Subsequently we have a decreasing exponential behaviour.



(a) In this image are shown the distributions of how much time two particles are close together. The distributions are in function of the occupancy and of the radius ratio. Every value of the time length corresponds to 0.15 seconds of simulation time. In this image we show three of the distribution obtained varying only the radius ratio. We can see a clear negative exponential behaviour, for this we show the same distribution in a logarithmic scale in the Fig. (b)



(b) The distribution shown in this image are the logarithmic scale of the distribution in the previous image, we can see that as the radius ratio area increases (from orange to blue to violet) the time that the particle tend to not change too much.

Figure 4.9

It is evident that as the area occupied by the particles increases, the time the molecules tend to stick close to each other increase visibly too. Meanwhile

Occupancy	0.3	0.4	0.5
Slope	-0.0246	-0.0176	-0.0106

Table 4.1: Values of the Slope for the distribution shown in Fig. 4.8. We can see a decrease of the negative exponential of the length of the time the particle spend close to each other as the occupancy increases.

Radius Ratio	0.25	0.30	0.35
Slope	-0.0196	-0.0176	-0.0167

Table 4.2: Values of the Slope for the distribution shown in Fig. 4.9. We can see a less steep decrease of the negative exponential, in respect to the previous table, as the radius ratio increases.

as the Radius ratio increases there is again a growth of the time the molecules spend together, but it is less evident.

We choose to interpolate the data to obtain the coefficient of the exponential behaviour. For interpolating we choose to use the semi-log distribution and select the data from when it starts to behave exponentially to when the value are not visited enough and they go to zero, as shown in Fig. 4.7. Since we chose to use the semi-log distribution, we will show the Slope and the Y Intercept of the line obtained trough the fit.

### Estimation of the Clustering Time with Dissipation

When two molecules bump one into the other the collision is rarely perfectly elastic and there is a little dissipation of energy.

For this reason we decided to repeat the simulation shown above with in addition a little dissipation between the collisions of the bigger spheres and a suitable reheating of the smaller particle ensuring that the temperature of our system would not drop too low.

Through the usage of the features of NOCS Elasticity and Resetter the task was easily done. Every time two bigger spheres hit each other we made them dissipate the 20% of their energy. Every time step of our simulation we calculated the total energy off all the spheres, both big and small, present. If the value of the total energy was inferior to the 95%, we set the energy of the smaller particles to a value which added to the value of the energy of the bigger particles was equal to the initial energy.

As we can see from the Fig. 4.10 when the dissipation is active in our simulation the exponential decay happens slower. Moreover the bulk value at the beginning of our distribution is reduced, in fact, introducing the dis-

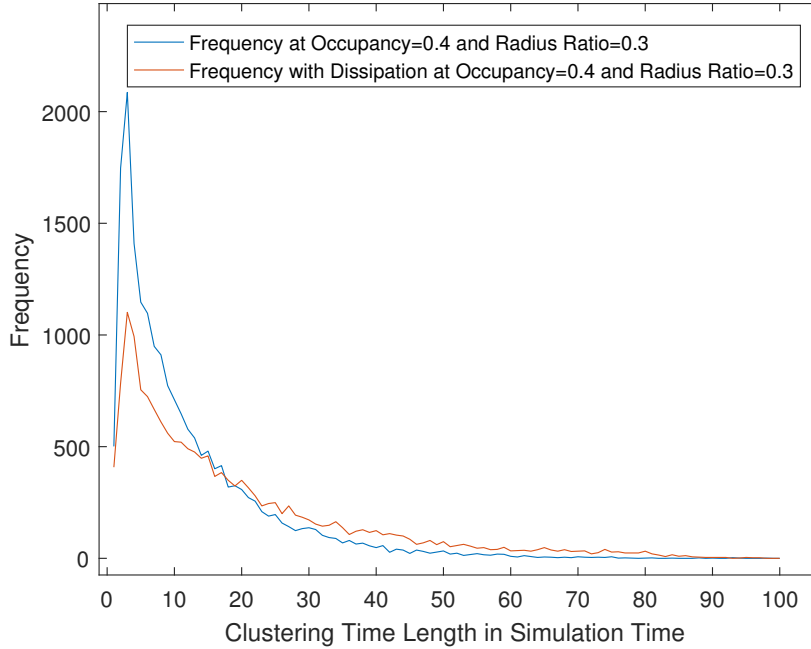
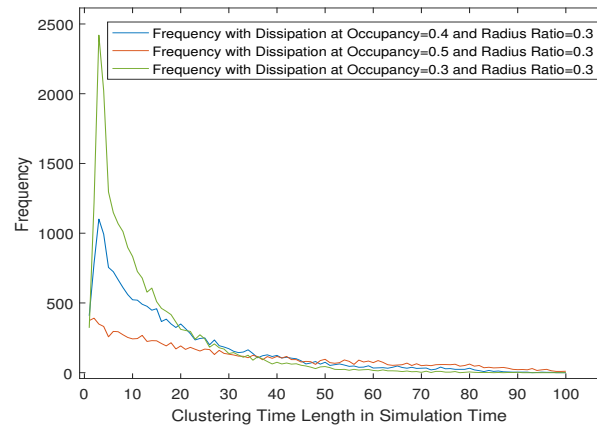


Figure 4.10: We show in this image the comparison of the distribution of the time length between the case without dissipation and the one with dissipation at the same conditions. Every value of the time length corresponds to 0.15 seconds of simulation time.

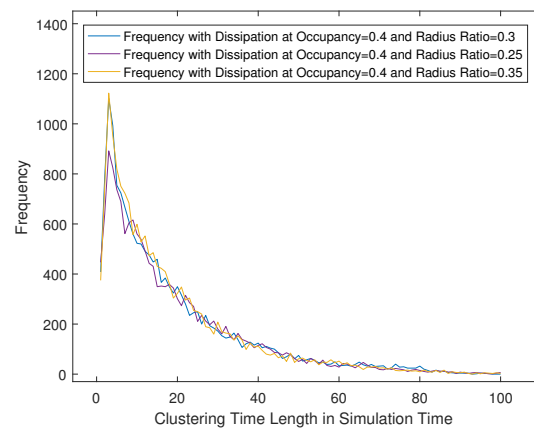
sipation, we were able to decrease the overestimate of the low length time intervals.

As we can see from the Tab. 4.3 and 4.4, the values of the negative exponential are reduced respect the simulations without dissipation. The order is kept, comparing the simulation with and without dissipation, in the values of the exponential with respect to the occupancy, while we can see an exchange of values with respect to the radius ratio.

This may be due to the fact that the potential shown previously have a more significant difference varying the occupancy, so the order is maintained, while the difference in the potentials in the case in which we vary the potential is smaller. Moreover the potential generated by bigger depletion agents, despite being a little smaller, has a longer range, so in the case without dissipation it may be more effective than the one generated by smaller depletants.



(a) In this image are shown the distributions of how much time two particles are close together when the dissipation is activated. In this image are shown the distribution varying the occupancy. Every value of the time length corresponds to 0.15 seconds of simulation time.



(b) In this image are shown the distribution varying the radius ratio. Every value of the time length corresponds to 0.15 seconds of simulation time.

Figure 4.11

Occupancy	0.3	0.4	0.5
Slope	-0.0166	-0.0107	-0.0056

Table 4.3: Values of the Slope for the distribution shown in Fig. 4.11a. We can see again a decrease of the negative exponential of the length of the time the particle spend close to each other as the occupancy increases. Furthermore the coefficient of the negative exponential is significantly decreased compared to the values of the simulation without dissipation.

Radius Ratio	0.25	0.30	0.35
Slope	-0.0103	-0.0107	-0.0117

Table 4.4: Values of the Slope for the distribution shown in Fig. 4.11b. In this case there is an inversion of the trend compared to the case of the simulation without dissipation. In fact the potential generated by the particles with a bigger radius is a little smaller, but it acts in a longer range, probably with dissipation the effect is more noticeable.



# Chapter 5

## Conclusive Remarks

The entropic forces may have played a fundamental role in the shaping of some kind of macromolecules and of the proteins, in particular amino acids. Since the systems of interest are extremely complicated and even if this forces and excluded volume effects exist and they may facilitate an entrapment due to a potential well, they may not determine it. It is difficult to determine an actual result for understanding how the proteins truly developed, for this reason it is important to develop our knowledge through computational simulations.

In this thesis project we studied how a particular molecule, formed by three spheres equidistant in two dimension is subject to the effects of excluded volume and we tried to understand how the shape of a molecule gives us information on its behaviour when it is subject to collisions.

We also studied in a system of binary hard sphere mixture how the potential behaves in function of the density of the spheres and of the radius ratio between the two spheres involved, through dynamical simulations. Moreover we estimated the distribution of the clustering time again in comparison with in function of the density of the spheres and of the radius ratio in a case where elastic collisions happened and in a case in which we let the spheres of interest dissipate part of their energy, keeping the temperature constant. Finally we made a comparison for understanding the parameters which can enhance the length of the clustering time.



# Appendix A

## Recent experimental discoveries

### A.1 How the molecules move along a temperature gradient in aqueous solutions

It has been known since the end of the 19th century, experimentally, that particles may move along along a temperature gradient. This phenomenon is known as the Soret Effect, thermodiffusion or thermophoresis. Particles usually move from regions with higher temperature to regions with lower temperature, but the inverse Soret effect exists too. The Soret effect theoretically is not yet clearly understood, recent studies [4] give us an interesting insight for the Soret Effect when the gradient of the temperature is sufficiently small.

Let us start with a straightforward theoretical explanation of thermodiffusion. For diluted concentrations, it is generally assumed that the drift velocity due to thermodiffusion depends linearly on the gradient of the temperature  $\Delta T$ .

In fact if we combine the drift of the thermophoresis with the diffusive back flow we have the drift current density

$$j = j_D + j_{TD} = -D\nabla c - D_T c \nabla T \quad (\text{A.1.1})$$

where  $D$  is the diffusion coefficient due to the diffusive back flow,  $\nabla c$  is the molecule concentration gradient  $D_T$  is the thermodiffusion coefficient and  $\nabla T$  is the temperature gradient. It happens that  $j = vc$ , and so, as it was already stated

$$v = -D_T \nabla T. \quad (\text{A.1.2})$$

When the system is in the steady the sum of the two currents compensate, and thus  $j = 0$ , this bring us to the following equation, when the difference

in temperatures are small

$$\frac{dc}{c} = -S_T dT \quad (\text{A.1.3})$$

with  $S_T = D_T/D$ , which is the Soret coefficient.

If the Soret coefficient is constant integrating the previous equation we obtain

$$\frac{c(\vec{x})}{c_0(\vec{x}_0)} = e^{-S_T(T(\vec{x})-T_0(\vec{x}_0))} \quad (\text{A.1.4})$$

and  $\vec{x}_0$  is an arbitrarily defined location, with a temperature  $T_0$  and a concentration  $c_0$ . As we can see from the previous equation the dependence between the concentration and the temperature is exponential, and the concentration  $c$  depends only on the difference  $T - T_0$ .

To reach the position  $\vec{x}$  from  $\vec{x}_0$  in a steady state let us consider to concatenate many arbitrary small regions by diffusion, sufficiently small regions so that it is possible consider each region to have a local equilibrium.

We can express the ratio of the concentration of the final region  $c_N$  and the initial region  $c_0$  as a sequence of products of local concentration ratios of neighbouring regions, expressed by local laws of thermophoresis

$$\frac{c_N}{c_0} = \prod_{i=1}^N \frac{c_i}{c_{i-1}} = \prod_{i=1}^N 1 - S_T(T_i - T_{i-1}) \quad (\text{A.1.5})$$

If we assume a equal spacing in temperature between the various regions  $\Delta T = (T_N - T_0)/N$ , for a fairly large  $N$  we can apply the limit definition of the exponential function to equ. (A.1.5) and obtain

$$\frac{c_N}{c_0} = \left[ 1 - S_T \frac{T_N - T_0}{N} \right]^N \rightarrow e^{-S_T(T_N - T_0)} \quad (\text{A.1.6})$$

Even if the system globally is in a non equilibrium state, local thermodynamic equilibrium of many regions may assemble in a global steady state.

In the work of Duhr and Dieter the previous relation was put to test using microfluidic fluorescence. The gradient of the temperature was generated through an infrared laser at a wavelength of 1480 *nm* with power used usually at 25 *mW*. A water chamber was formed using polystyrene slides of 10  $\mu m$  thickness. A 32 $\times$  air objective put in a fluorescence upright microscope was used for the imaging.

The spot heated by the laser had a  $\Delta T = 8 K$  with a full width of 40  $\mu m$ .

The thermophoresis of polystyrene beads with a diameter of 200 *nm* was measured. The beads were diluted to 0.02% solid in 1 *nM* Tris buffer. The

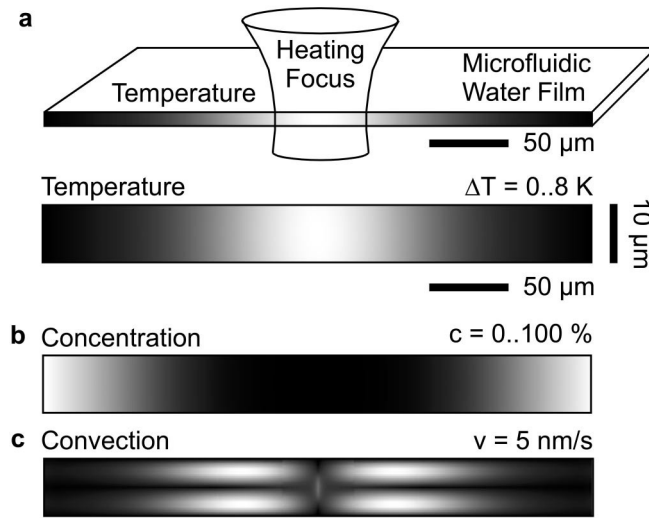


Figure A.1: This image shows some of the specific of the experimental approach. (a) A film of water is surrounded by polystyrene slides. The low thermal conduction due to the walls and the thin water film allows a temperature profile which is independent of the thickness. (b) As a consequence also the depletion profile due to the thermophoresis shows no dependence on the thickness. (c) Convection has negligible velocity, at most of  $5 \text{ nm/s}$ , due to thin film of water and broad heating focus.

thermophoretic properties of the system stated above were measured for a small  $\Delta T$  of  $1.2 \text{ K}$ , bringing to the results of  $D_T = 1.4 \mu\text{m}^2/(\text{sK})$  and  $D = 2.1 \mu\text{m}^2/\text{s}$  and thus  $S_T = 0.7 \text{ K}^{-1}$ .

For obtaining the concentration of particles the luminosity of 50 images were averaged, each image was obtained with an exposure time of 10 seconds and it was recorded with 12-bit resolution.

The protocol for collecting the images was formed by three steps

- The first step was to collect the images before the laser started to heat the system in the decided spot.
- The second images are obtained after a twenty minute of laser heating, in a steady state.
- The last kind of images are obtained after 20 minutes of back-diffusion, needed for correcting the fluorescence bleaching of the beads.

The result of the images obtained is that the bleaching could be corrected linearly and the possible inhomogeneous illumination was removed by dividing with the images obtained before the heating of the system. The profiles

of the radial concentration were obtained from the average of the group of images. The background fluorescence was removed in respect of the central depleted region.

The experiment was simulated using a finite element calculation taking into consideration Navier-Stokes flow superposed with thermal expansion, heat transfer, gravity, molecule diffusion and thermophoresis. The temperature profile of the film of water is flat due to the low thermal conductivity of the walls of the chamber in polystyrene (Fig. A.1a). Small deviation from a constant  $z$  profile of both temperature and concentration compensate in the first order. The simulation does not underline a disturbance of the profile of the concentration of beads caused by the thermal convection (Fig. A.1b) and this happens because the maximum speed due to thermal convection is only of  $5 \text{ nm/s}$ .

The radial temperature distribution of the system was measured using the BCECF fluorescence (Fig. A.2a). The average of the temperature (linear) and of the concentration (logarithmic scale) in function of the radius is shown in Fig. A.2d. The exponential dependence between the temperature and the concentration has a Soret coefficient of  $S_T = 0.72/k$ , quite close to the value measured for the system at a smaller temperature interval. The beads in consideration may have a Soret coefficient with a small temperature dependence, but the experimental result may be equally explained with or without it.

Equations (A.1.5), (A.1.6) and the division in small region of local equilibrium may be put to test may be put to test. The temperature and the concentration locally do not present an abrupt change and a linearized Boltzmann distribution holds and when this happens small concentration changes  $dc$  are related to small Gibbs free energy differences  $dG$ :

$$\frac{dc}{c} = -\frac{dG}{kT} = -S_T dT. \quad (\text{A.1.7})$$

As we have showed before, the local Boltzmann law is related to the Soret coefficient  $S_T$ , and this permits to connect it with the Gibbs free enthalpy  $G$  (in the case of constant pressure and nearly constant temperature).

The finite size of the beads limits the subdivision in local equilibrium system. The steepest temperature gradient that the authors were able to recreate in this experiment was of  $\Delta T = 0.1 \text{ K}/\mu\text{m}$ , and in this case the energy difference over the radius  $a$  of a particle is

$$a \times \Delta G = a \times S_T \Delta T kT = 0.01kT. \quad (\text{A.1.8})$$

The particle thermal fluctuation is known to be  $kT/2$ , and the asymmetry across the particle is only the 2% of this value.

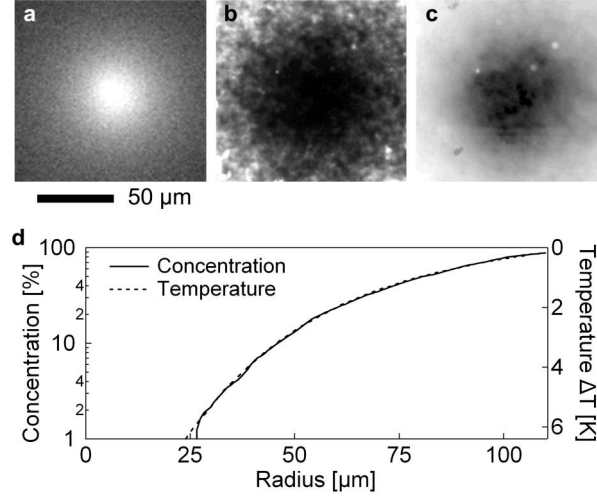


Figure A.2: (a) Measure of the temperature through the BCECF fluorescence. (b) A single image of the depletion of the polystyrene beads due to the thermophoresis. (c) Logarithmic bead concentration image obtained through the average of 50 single images and after illumination and bleach correction. (d) The average of the concentration (logarithmic) and of the temperature in function of the radius.

The total possible energetic difference in the experiment was

$$\Delta G = k\bar{T} \ln(c_{min}/c_{max}) = 4.6k\bar{T},$$

well beyond local equilibrium. Thus the partition applied in equations (A.1.5) and (A.1.6) can be applied for  $N = 4.6/0.01 = 460$  times, and this is a sufficient converged exponential steady state.

It's interesting and based on actual experimental evidence to describe the thermophoretic steady states by a Boltzmann distribution with local thermodynamic equilibrium:

$$\frac{c}{c_0} = e^{-S_T(T-T_0)} = e^{-\frac{G(T)-G(T_0)}{k\bar{T}}} \quad (\text{A.1.9})$$

There is a linear relation between  $S_T$  and  $G(T)$ , introduced in equ. (A.1.7), this bring us to the prediction on how the size of the particles affects the thermophoresis. Since for solid particles only the salvation energy at their surface is temperature dependant thus the Soret coefficient must scale with particle surface area. We have that  $D \propto a^{-1}$ ,  $D_T$  scales with particle radius and thus

$$S_T \propto \frac{\partial G}{\partial T} \propto a^2, \quad D_T \propto D \frac{\partial G}{\partial T} \propto a. \quad (\text{A.1.10})$$

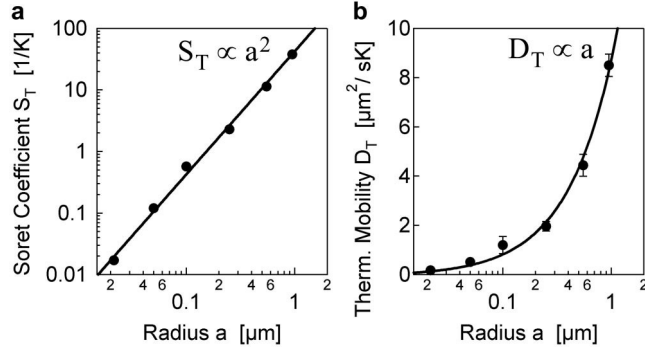


Figure A.3: (a) The trend of the Soret coefficient of beads in function of the radius of its beads. (b) The thermophoretic coefficient  $D_T$  scales linearly with the radius of its beads, in accordance with how the Soret coefficient behave.

The authors measured the Soret coefficient for some beads of polystyrene of various sizes, the radii considered varied from 200 nm to 1  $\mu\text{m}$ . The measurement obtained match well with equ. (A.1.10), as we can see in Fig. A.3. For larger particles the equilibrium cannot be assumed, since the energetic difference is bigger than  $kT$ .

To summarise the results shown so far, the authors collected evidence in support of describing, for opportune condition, the thermophoresis as a local thermodynamic equilibrium.

If the system has a moderate thermal gradient, the depletion due to thermophoresis has an exponential steady state distribution over two order of magnitude and the Soret coefficient, for solid particles, has a scaling law in function of the radius of the beads considered.

Another article [5] start from the result shown above and look further into this subject. The starting point is in equation (A.1.7), in particular the relation between the Gibbs free energy and the Soret coefficient.

An infinitesimal change in the Gibbs free energy can be expressed as  $dG = -SdT + Vdp + \mu dN$ , thus for a single particle if the pressure remains constant we have that the Soret coefficient is equal to  $S_T = -S/kT$ .

# Dedications

Vorrei ringraziare Chiara per essermi stata vicina in quest'ultimo anno di tesi, anche se non sempre è stato facile, per avermi spronato e perché è stato un anno molto bello .

Vorrei ringraziare mia madre e mio padre padre perché senza di loro non sarei qui. Ringrazio mio fratello don Davide per i preziosi consigli. Grazie anche agli altri familiari che mi hanno sempre supportato.

Vorrei ringraziare don Mario e la famiglia Marchesini per avermi ospitato più di un anno e vorrei ringraziare tutti gli strani fratelli e sorelle delle case canoniche e tutti gli amici che ruotano attorno a via Massarenti 59, in particolare Nilton.

Un grazie speciale a tutti gli studenti anonimi che si incontrano in giro sia a Bologna che a Modena, lo studio con voi vicino è stato meno pesante.

Grazie agli amici di via del Pelo, al Moto Relativo, di Soliera, ai Nomore.

Un grazie alla gente del Mismo, del Gim di Padova perché mi hanno fatto vedere un mondo diverso. Grazie inoltre alle persone con cui ho condiviso il viaggio a Nairobi di quest'estate.

Grazie all'associazione Improgramelot e ai compagni di viaggio nell'improvvisazione i BamBoss.

Ringrazio Matteo Monti per la disponibilità nello spiegarmi come utilizzare il suo programma, il professor Bazzani, i suoi dottorandi e post-doc perché mi hanno sempre aiutato nei momenti di dubbio.



# Bibliography

- [1] Sho Asakura and Fumio Oosawa. “Interaction between Particles Suspended in Solutions of Macromolecules”. In: *Polymer Science XXXIII* (1958), pp. 183–192.
- [2] Jayanth R. Banavar and Patrick J. Fleming Amos Maritan George D. Rose. “A backbone-based theory of protein folding”. In: *PNAS* 103 (2006), pp. 16623–16633.
- [3] Jayanth R. Banavar and Amos Maritan. “Geometrical approach to protein folding: a tube picture”. In: *REVIEWS OF MODERN PHYSICS* 75 (2003).
- [4] Stefan Duhr and Dieter Braun. “Thermophoretic Depletion Follows Boltzmann Distribution”. In: *PHYSICAL REVIEW LETTERS* 96 (2006), p. 168301.
- [5] Stefan Duhr and Dieter Braun. “Why Molecules Move Along a Temperature Gradient”. In: *Proceedings of the National Academy of Sciences of the United States of America* (2007), pp. 19678–82.
- [6] Henk N.W. Lekkerkerker and Remco Tuiner. *Colloids and the Depletion Interaction*. Springer, 2011.
- [7] Matteo Monti and Carlo Emilio Montanari. *Getting started with NOCS*. URL: <https://github.com/matteomonti/nocs/tree/master/docs>.
- [8] Phil Attard Ronald Dickman and Veronika Simonian. “Entropic Forces in Binary Hard Sphere Mixtures: Theory and Simulation”. In: *The Journal of Chemical Physics* (1998), pp. 107, 205.